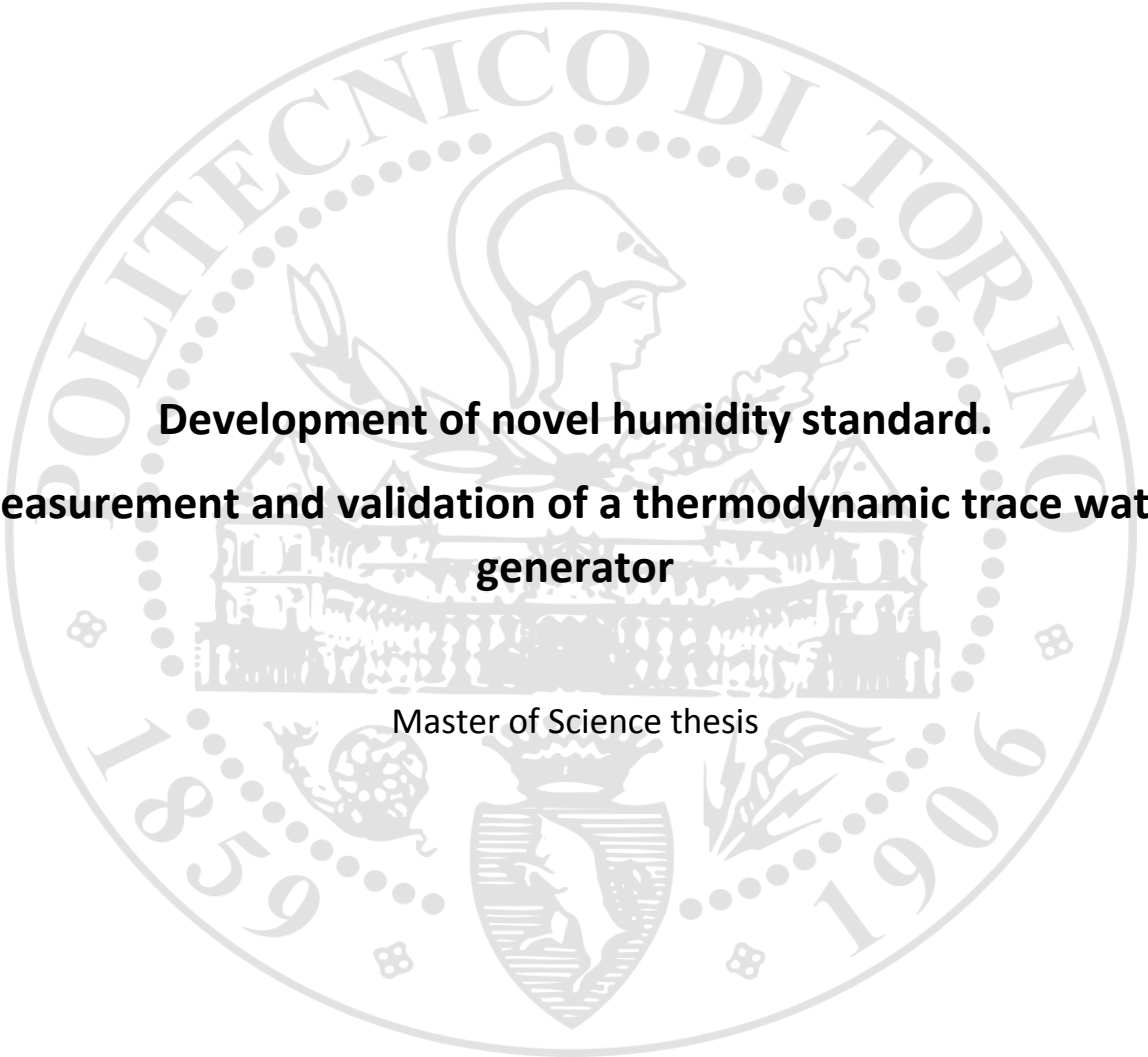


POLITECNICO DI TORINO

Master of Science in

Mechanical engineering



**Development of novel humidity standard.
Measurement and validation of a thermodynamic trace water
generator**

Master of Science thesis

Rezvaneh Nobakht Parashkouhi

POLITECNICO DI TORINO

Master of Science in
Mechanical engineering



Development of novel humidity standard
Measurement and validation of a thermodynamic trace water
generator

Master of Science thesis

Student:

Rezvaneh Nobakht Parashkouhi

Student N: s257684

Supervisors:

Prof. Vito Fericola

Dr. Rugiada Cuccaro

Academic year 2020-2021

to my family;

Contents

1. Introduction	Error! Bookmark not defined.
2. Humidity measurements	Error! Bookmark not defined.
2.1 Definitions related to humidity	Error! Bookmark not defined.
TEMPERATURE	Error! Bookmark not defined.
DEW POINT TEMPERATURE	Error! Bookmark not defined.
FROST POINT TEMPERATURE	Error! Bookmark not defined.
WET BULB TEMPERATURE (T_w)	Error! Bookmark not defined.
PRESSURE.....	Error! Bookmark not defined.
DALTON'S LAW	Error! Bookmark not defined.
ENHANCEMENT FACTOR (f)	Error! Bookmark not defined.
RELATIVE HUMIDITY (RH %).....	Error! Bookmark not defined.
ABSOLUTE HUMIDITY AND VOLUMETRIC CONCENTRATION	Error! Bookmark not defined.
2.2 Humidity sensors	Error! Bookmark not defined.
2.2.1 Measurement requirements	Error! Bookmark not defined.
<i>Performance</i>	Error! Bookmark not defined.
<i>Output, readout</i>	Error! Bookmark not defined.
<i>Hazardous areas</i>	Error! Bookmark not defined.
<i>Robustness</i>	Error! Bookmark not defined.
2.2.2 Type of instruments	Error! Bookmark not defined.
<i>Mechanical</i>	Error! Bookmark not defined.
<i>Wet and dry bulb (psychrometer)</i>	Error! Bookmark not defined.
<i>Acoustic</i>	Error! Bookmark not defined.
<i>Chilled mirror</i>	Error! Bookmark not defined.
<i>Resistive type</i>	Error! Bookmark not defined.
<i>Capacitive sensor</i>	Error! Bookmark not defined.
<i>Optical sensors</i>	Error! Bookmark not defined.
<i>Cavity ring down spectrometer</i>	Error! Bookmark not defined.
<i>Piezoresistive Sensors</i>	Error! Bookmark not defined.
3. Humidity standards	Error! Bookmark not defined.
3.1 Measurement traceability	Error! Bookmark not defined.
3.1.1 The International System (SI) of units	Error! Bookmark not defined.

3.1.2 Calibration and Traceability	Error! Bookmark not defined.
3.2 Humidity generator	Error! Bookmark not defined.
<i>Gravimetric hygrometer</i>	Error! Bookmark not defined.
<i>Two flows generator</i>	Error! Bookmark not defined.
<i>Two temperature generator</i>	Error! Bookmark not defined.
<i>Two-pressure generator</i>	Error! Bookmark not defined.
<i>Hybrid method</i>	Error! Bookmark not defined.
<i>Diffusion tube generator</i>	Error! Bookmark not defined.
4. A novel humidity standard	Error! Bookmark not defined.
4.1 Introduction	Error! Bookmark not defined.
4.2 Design of a trace water generator	Error! Bookmark not defined.
4.3 Experimental evaluation of the generator performance	Error! Bookmark not defined.
5. Uncertainty evaluation	Error! Bookmark not defined.
5.1 Introduction	Error! Bookmark not defined.
5.2 Uncertainty analysis of the trace water generator	Error! Bookmark not defined.
6. Conclusions	Error! Bookmark not defined.
Appendix	Error! Bookmark not defined.
A.1 Bath temperature stability	Error! Bookmark not defined.
A.2 Experimental results of generator efficiency	Error! Bookmark not defined.
A.3 Uncertainty analysis	Error! Bookmark not defined.
References	Error! Bookmark not defined.

1. Introduction

Water is everywhere, whether in solid (ice), liquid (water), or gaseous form (water vapour). Water in a gaseous state is called humidity. It is present everywhere in the atmosphere, even in very dry areas.

Measuring humidity is important because it plays a key role in the quality of products and the cost of processing materials, as well as in human comfort. In warehouses, for example, controlling humidity protects against corrosion or preserves sensitive materials such as steel coils or food and dry milk. Vegetables are about 90 % water, and if 5 % of it is lost, the commercial value is lost. Therefore, it is necessary to maintain a low temperature and high humidity to reduce water evaporation. On the other hand, a high temperature and high humidity increase the risk of microbial growth, which causes the vegetables to rot.

Paper also contains about 5 % to 7 % water. Humidity control is necessary to reduce expansion and contraction of paper due to evaporation of water. In addition, humidity helps prevent static electricity that causes paper jams. If the humidity in the computer room is too high, condensation can occur, causing a short circuit. If the humidity is too low, static electricity can occur, which can cause the electronic device to shut down or be damaged.

Humidity is defined as the presence of water vapour in the air or other gases. Humidity depends on the temperature and pressure of the system. The same amount (mass or mole) of water vapour will result in higher humidity in cool air than in warm air. Therefore, to achieve controlled humidity, temperature and pressure must be controlled.

A number of manufacturing processes are affected by trace amounts of water vapour in pure and process gases. It is important for operators of such processes to continuously monitor the water vapour content in these gases prior to delivery to the customer to ensure the integrity and safety of the equipment.

Water vapour is unique among process contaminants. It affects electrical, chemical, thermo-physical, and mechanical properties, as well as electrical conductivity, making its measurement critical and difficult. It can also lead to corrosion and decomposition. Pure gases such as Ar, N₂, H₂ or O₂ are used in a variety of industries: medical, food and beverage, petrochemical or chemical. Depending on the application, purity requirements can range from percent to parts per million.

There are many analytical methods for determining trace water vapour, all of which require regular and traceable calibration. Humidity can be fully described by a single parameter if the gas pressure and temperature are known. For this reason, many national humidity laboratories have chosen dew point temperature as their primary humidity parameter. As for the realisation of a dew point temperature scale, a dew point generator provides a simple source of traceability over a wide range and with an excellent uncertainty level¹.

INRIM-03 is a novel humidity standard, an ultra-low dew point generator designed to extend Italian humidity calibration and measurement capabilities (CMCs) to a few parts per billion of water. It can generate a humid gas stream with a water vapour content of up to 15 parts per billion. This generator is among the few in the world that can operate at freezing point temperatures as low as -99 °C and at sub-atmospheric pressures (200 hPa) regardless of gas flow rate, which can vary from 1.5 l·min⁻¹ to 7 l·min⁻¹.

The generator system described above is the subject of this thesis. The experimental results of the work are intended to support the validation of the individual components of the measurement uncertainty and to develop a comprehensive uncertainty budget for the frost point temperature T_{fp} and the water vapour mole fraction x_w produced by the generator.

The experimental results of the work have shown that the INRIM-03 humidity generator can produce a humid gas stream with a frost point temperature between -99 °C and -75 °C with a minimum combined measurement uncertainty of 0.02 °C or, equivalently, a water vapour mole fraction between $34 \cdot 10^{-9}$ mol·mol⁻¹ and $6 \cdot 10^{-6}$ mol·mol⁻¹ with a minimum combined uncertainty of $3 \cdot 10^{-9}$ mol·mol⁻¹.

2. Humidity measurements

2.1 Definitions related to humidity

TEMPERATURE

The degree of hotness or coldness of a body. The units are Celsius (°C) and kelvin (K). The relation between them are:

$$T/K = 273.15 + T/°C$$

DEW POINT TEMPERATURE

The temperature to which a volume of a gas must be cooled such that it becomes saturated with respect to the liquid water.

FROST POINT TEMPERATURE

The temperature to which a volume of gas must be cooled, such that it becomes saturated with respect to ice.

WET BULB TEMPERATURE (T_w)

When unsaturated air passes through a moist thermometer, at a given point the rate of heat transfer by convection and conduction from the air to the surface is equal to the rate of latent heat of evaporation from the surface. This equilibrium temperature is the wet bulb temperature.

PRESSURE

Pressure is defined as the stress or force that is applied uniformly in all direction. It's the force per unit of the area. The unit is the pascal (Pa) ($\frac{1\text{ N}}{\text{m}^2} = 1\text{ Pa}$).

The pressure most commonly used is the atmospheric or barometric pressure $P_{\text{barometric}}$. In industry, pressure is measured in terms of vacuum, which is equivalent to absolute pressure P_{abs} . So:

$$P_{\text{abs}} = P_{\text{gauge}} + P_{\text{barometric}}$$

DALTON'S LAW

In the ideal gas the relation between pressure, temperature and volume are defined as:

$$PV = nRT$$

where P is the absolute pressure, V is the volume, n is the number of the moles of the gas, T is the absolute temperature and R is the universal gas constant.

Dalton supposed that if he had a mixture of gases, the total pressure of the mixture, P_{tot} , will be equal to some of the partial pressure of the component gases, P_i :

$$P_{\text{tot}} = \sum P_i$$

Once moisture is in the gas mixture, it behaves according to the principle of the gas law and exerts a partial pressure in the gas mixture according to Dalton's law. Based on this law, measuring humidity basically boils down to measuring the partial pressure of the water vapour component of the gas mixture.

ENHANCEMENT FACTOR (f)

The above statement about the behaviour of a gas is considered as the "ideal gas behaviour". To get closer to reality, a small pressure-dependent correction may be necessary: the "water vapour enrichment factor". The saturation vapour pressure over a surface in the pure condensation phase depends strictly on the temperature. However, when a second gas is passed over the surface of the water, the saturation vapour pressure increases. This increased vapour pressure (the effective vapour pressure) is different from the saturation vapour pressure of the pure phase and is expressed by:

$$f = \frac{x_w P}{e_s}$$

with f – enhancement factor, x_w – mole fraction of water vapour in the saturated mixture, P – total pressure above the surface of the condensed phase (liquid or solid), e_s – pure phase saturation vapour pressure.

RELATIVE HUMIDITY (RH %)

Relative humidity is the ratio of the actual partial vapour pressure (e) to the saturation vapour pressure of the gas (e_s)

$$RH \% = \frac{e}{e_s} 100 \%$$

ABSOLUTE HUMIDITY AND VOLUMETRIC CONCENTRATION

Absolute humidity is defined as water vapour density and is expressed as water vapour mass per unit volume of dry air.

$$A_w = \frac{g}{m^3} = 216.7 \frac{e_w}{T_a + 273.16} = 216.7 \frac{e_i}{T_a + 273.16}$$

In the equation, e_i and e_w are the vapour pressure with respect to the ice and water and T_a is the ambient or dry bulb temperature.

Amount fraction (in mass or in volume) of water is also used to describe concentrations. Parts per million by weight (ppm_w) is the number of units of mass of a contaminant per million units of total mass. Parts per million by volume (ppm_v) is often used to describe concentrations of trace contaminants in air and other gases. In this case the conversion to ppm_w depends on the molecular weight of the contaminant. The relation between the water vapour content expressed in part per millions by volume (ppm_v) and part per millions by weight (ppm_w) is:

$$PPM_v = 10^6 \cdot e/P - e = \frac{\text{Partial pressure of } H_2O}{\text{Total pressure} - \text{Partial pressure of } H_2O} \cdot 10^6$$

$$PPM_w = \frac{\text{mass of water vapor}}{\text{mass of carrier gas}} \cdot 10^6 = PPM_v \cdot \frac{\text{Molecular weight of water vapor}}{\text{Molecular weight of carrier gas}}$$

2.2 Humidity sensors

A humidity sensor is an electronic device that measures the humidity in its environment and converts it into an electrical signal.

2.2.1 Measurement requirements

Relative or absolute

Relative humidity (RH) sensors and absolute humidity (AH) sensors. Relative humidity is the ratio of the reading humidity at a given temperature to the maximum amount of humidity for air at the same temperature. To determine the relative humidity the sensor measure the temperature. In contrast, absolute humidity is measured without reference to temperature.

Range (humidity and other variables)

Different types of measurement are used depending on the range of humidity. To select the best device, the operating ranges of temperature, flow rate, and pressure must be known. For example, if the sensor is used at elevated pressure, the design of the device may be as important as the operating principle. On the other hand, for some types of measurements, it may be necessary to correct the results if the pressure varies.

Performance

To obtain a reliable measurement, you must establish criteria for sensitivity, stability (in the sense of repeatability or reproducibility), uncertainty, response time, resolution, linearity, or hysteresis.

Output, readout

The result of the sensor may be displayed as a digital number or by a needle on a numbered scale. It can be output as an electrical voltage or current signal (analogue output). The measured values can be displayed continuously or at intervals. The instrument can record the measured values on a paper chart.

The measured values can be stored electronically in the instrument's memory or downloaded directly to a computer in digital form via a "serial connection".

Hazardous areas

In areas where there is some danger, such as an explosive atmosphere, appropriate precautions must be taken. For example, sampling gas to remote probes may reduce the risk in some cases, while other sensors can be designed to be "intrinsically safe" by limiting the electrical output to a value low enough not to ignite the atmosphere. Where this is a problem, appropriate intrinsic safety certification should be sought.

Robustness

Both hygrometer sensors and housings have varying degrees of resistance to condensation, desiccation, extreme temperatures, dust, chemical or other contamination, vibration, or even simple handling.

2.2.2 Type of instruments

Mechanical

Early humidity sensors used natural materials like silk, hair or paper as the mechanical sensing element; the material shrank when dry because of low relative humidity and expanded when the humidity was high. ²

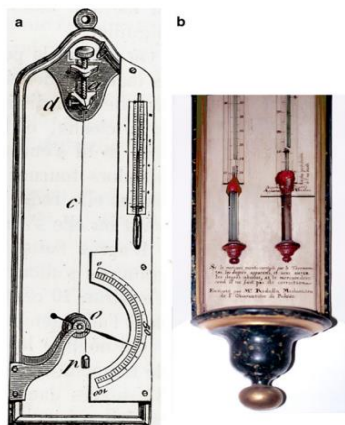


Figure 2.1. Hair hygrometer².

Wet and dry bulb (psychrometer)

An instrument to measure the dew point, relative humidity, and vapour pressure. It essentially consists of two ordinary, accurate, mercury thermometers. One has thin muslin wrapped around it and is kept wet; it is called a wet bulb thermometer. The other is a dry-bulb thermometer. The dry bulb thermometer shows the current temperature, whereas the wet-bulb shows a lower temperature. Relative humidity can be estimated from the tables below or alternatively from a psychrometric diagram or chart.



Figure 2.2. Wet bulb hygrometer.

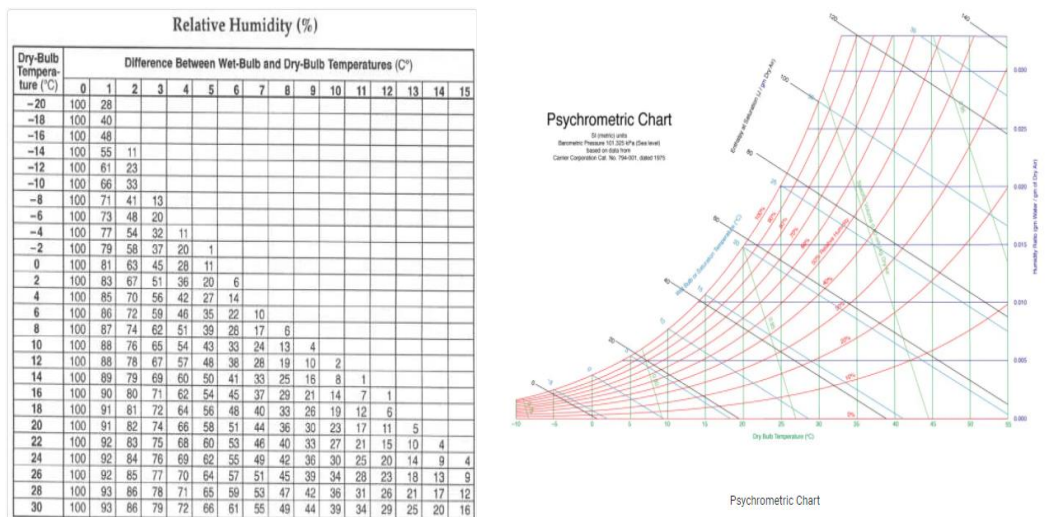


Figure 2.3. Psychrometric table and chart.

Acoustic

An acoustic relative humidity sensor for air-steam mixtures in duct flow is designed and tested. The measurement device is capable of measuring line averaged values of gas velocity, temperature and relative humidity (RH) instantaneously, by applying two ultrasonic transducers and an array of four temperature sensors. The speed of the sound, c , can be calculated as³:

$$c = \frac{L_t}{t_m}, t_m = \frac{t_1 + t_2}{2}$$

where t_m is the transit time averaged in second, L_t is the total length of the acoustic trajectory in meter between transducers Tr_1 and Tr_2 (Figure 2.4), t_1 is the transit time in downstream direction and t_2 the transit time in upstream direction in second. The problem here is for each pressure we need different plot³.

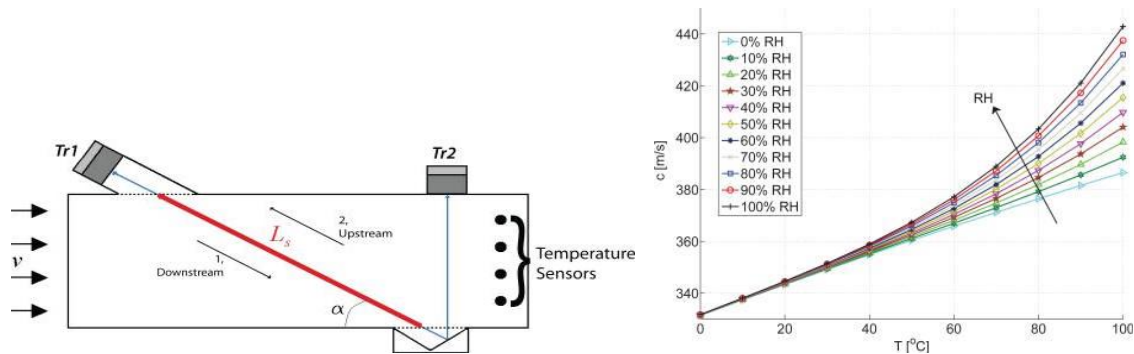


Figure 2.4. Internal view of an acoustic humidity sensor and the relative humidity plot³.

Chilled mirror

The measurement of the water vapor content of a gas by the dew-point technique involves chilling a surface, usually a metallic mirror, to the temperature at which water on the mirror surface is in equilibrium with the water vapor pressure in the gas sample above the surface. At this temperature, the mass of water

on the surface is neither increasing (too cold a surface) nor decreasing (too warm a surface). In the chilled-mirror technique, a mirror must be a good thermal conductive material such as silver or copper, and in order to prevent tarnishing and oxidation of the mirror it should be properly plated with an inert metal such as iridium, rubidium, nickel or gold. By a thermoelectric cooler the mirror is cooled down until dew just begins to form. A solid-state broad band light emitting diode beam, is aimed at the mirror surface and a photo detector monitors reflected light. After the gas flows over the chilled mirror, dew droplets form on the mirror surface and the reflected light is scattered, so the photo detector output also decreases. The detector by means of an analog or digital control system is connected to the thermoelectric heat pump which controls the mirror temperature at the dew point. A precision miniature platinum resistance thermometer (PRT) embedded on the mirror monitors the mirror temperature at the generated dew point⁴.

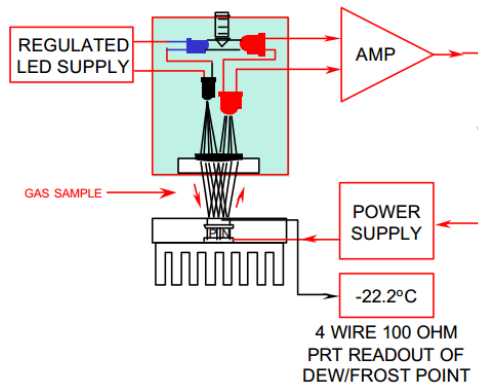


Figure 2.5. Schematic of the chilled mirror⁴.

Resistive type

Resistive humidity sensors measure the change in electrical resistance or the impedance of a hygroscopic medium such as a conductive polymer, salt or treated substrate.

Resistive sensors are based on a bifilar winding which consists of four layers like: substrate, inter digital electrode, humidity sensitive film and protective layer. After deposition of a hygroscopic polymer coating,

their resistance changes inversely with humidity. Ceramics, polymers and electrolytes are commonly used material for resistive type sensor. They are small, cheap, provide high sensitivity and stability, but on the other hand they can work in the limited range (typically 15 % to 95 %) and have high temperature dependency⁵.

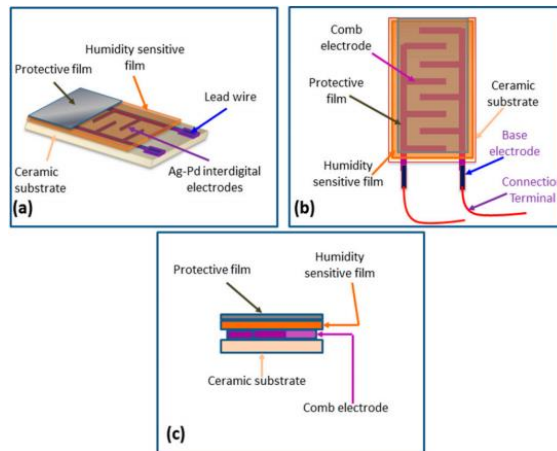


Figure 2.6. Different view of the resistive sensor⁵.

Capacitive sensor

Capacitive type humidity sensors are a function of the dielectric changes of thin films due to the absorption of water vapour. Their characteristics mainly depend on the hygroscopic nature of the material and the geometry of the electrode. Porous material like ceramics, silicon, silicon carbide, hygroscopic polymers and Al_2O_3 are utilized as humidity sensitive materials⁶.

The capacitive type can operate over a wide measurement range (0 % - 100 % RH) and at high temperatures (up to 200 °C), where the dependence on temperature is small. They are cheap but very stable and have a fast linear response with low hysteresis (less than 1 %). The only limitation is the distance between the electronics and the sensor. Also, electronics are required to convert capacitance to relative humidity⁶.

In this regards, capacitance C of all the parallel plate capacitive sensors follows a relation given by:

$$C = \frac{\epsilon A}{d}$$

where ϵ , A , d are the dielectric permittivity, the overlap area and the distance between two parallel plates respectively.

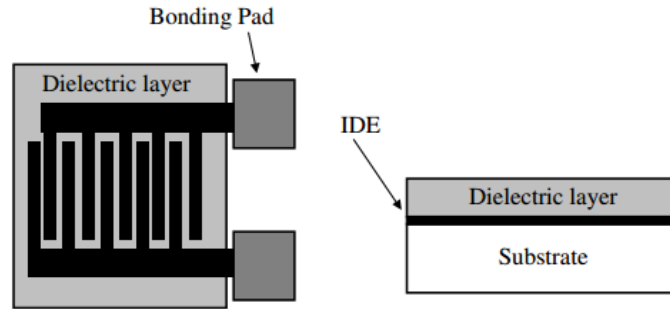


Figure 2.7. Capacitive humidity sensor⁶.

Optical sensors

There is a porous sensing element such as a silica-aerogel film, which is embedded on the optical fibres that absorb the water vapour molecules which leads to change the reflected optical power. So the main sensing principle of an optical humidity sensor is based on the change in reflected optical power due to the water molecules adsorbed on. The relative reflected power is a function of the refractive index of the media, n_i , the incidence angle and polarization of the incident wave. The reflected optical power, I , can be computed by the following equation where I_0 is the reference monitored optical power⁶:

$$I = I_0 \left[\frac{n_2 - n_1}{n_2 + n_1} \right]^2$$

These type of sensors have low cost and high sensitivity. Also they are robust, in small size and can be controlled remotely with low hysteresis. But they suffer from nonlinearity, inherent losses, and dispersion⁶.

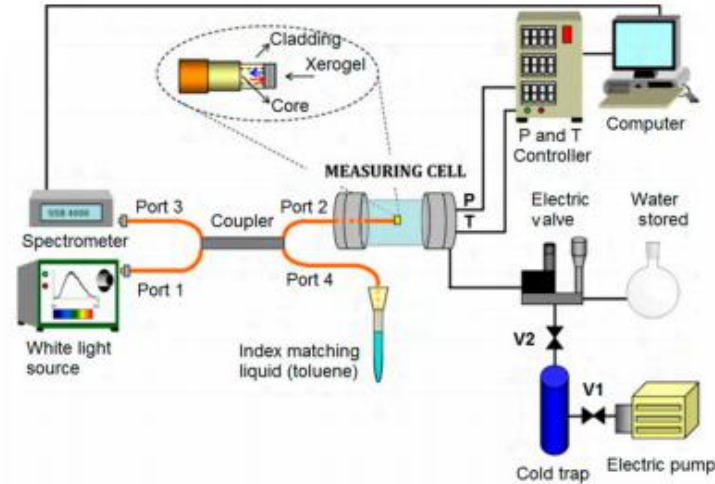


Figure 2.8. Schematic of an optical humidity sensor⁶.

Cavity ring down spectrometer

An empty cavity contains mirrors with a reflectivity of 99.99 % and a spacing of 0.1 m to 1 m, and a light detector. This high-finesse optical cavity contains the sample and the laser pulse is fired into it. The laser pulse is then monitored, decaying exponentially at a rate determined by the reflectivity of the mirrors and the length of the cavity. Thus, by measuring the time constant for the intensity decay of light stored in a cavity, called the ring-down time τ , the reflectivity of the mirrors can be determined. If the cavity contains an absorbing gas whose absorption frequency matches the wavelength of the laser beam, an additional optical loss occurs that causes a shortening of the ring-down time⁷. The ring down time is equal to:

$$\tau = \frac{t_r}{2[(1-R) + \alpha l_s]} \quad \alpha = \frac{1}{c} \left(\frac{1}{\tau_1} - \frac{1}{\tau_2} \right)$$

Where t_r is the round trip of the light pulse in the cavity, $(1-R)$ is the reflection loss, α is the absorption coefficient, l_s is the length, τ_1 is the ring down time for the cavity containing the absorbing species and τ_2 is the ring down time for the empty cavity.

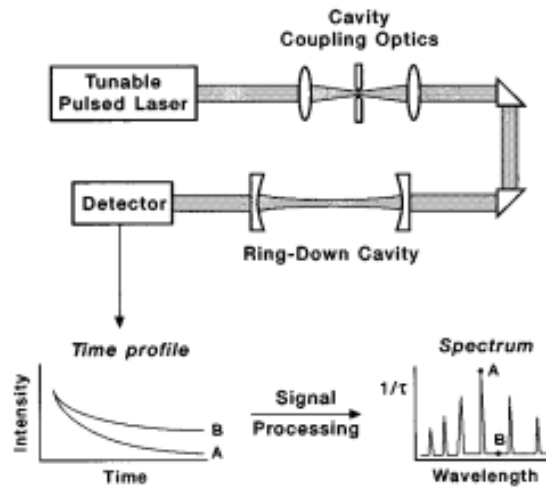


Figure 2.9. Schematic of the CRDS⁷.

During the tuning process a computer-controlled system compare the zero baseline which is the ring down time of an empty cavity to the present τ value which is dependent on the sample species concentration and find an equivalent zero baseline correction⁷.

By the Beer's Law the concentration of the sample species is directly calculated using the following equations⁷:

$$\tau_0 = \frac{d}{c(1-R)} \quad \tau(\nu) = \frac{d}{c(1-R + Nd\sigma(\nu))} \quad N = \frac{1}{c\sigma(\nu)} \left(\frac{1}{\tau(\nu)} - \frac{1}{\tau_0} \right)$$

where d is the cell length, R is the mirror reflectivity, $\sigma(\nu)$ is the absorption cross section and ν is the frequency.

Piezoresistive Sensors

Piezoresistive humidity sensors consists of a suspended structure coated with Polymer-based films that is a water-absorbent layer which its volume expands by absorption. This expansion leads to deform the polyimide-bridge substrate therefore causes a bending of the plate so this movement transformed into an output voltage by an integrated piezoresistive bridge. Independent of the shape of the diaphragm, the

coefficient of humidity expansion was shown to be approximately 60 to 80 *ppm* at different polyimide curing temperatures⁶. Significant temperature drift and providing the proper thermal coupling is the main concern during design procedure⁶.

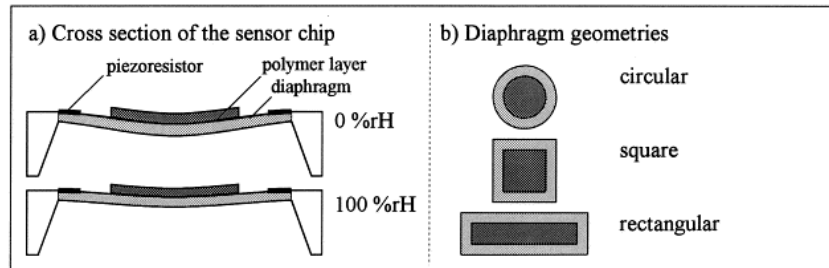


Figure 2.10. Piezoresistive humidity resistive sensor construction⁸.

3. Humidity standards

3.1 Measurement traceability

In metrology (the science of measurement), a standard is an object, system, or experiment that bears a defined relationship to a unit of measurement of a physical quantity. Standards are the fundamental reference for a system of weights and measures, against which all other measuring devices are compared. Long ago, the idea of a universal measuring system didn't exist. That was, until the 18th century where measurement became a cohesive system. The names for many units of measurement were borrowed from human morphology. For example, the foot, the hand, the pace, etc. Still, however, these units of measurement were not standardized. As industry and trade expanded across the world, the need became dire for a single standardized system of measurement. As trade was to flourish, a unified system was necessary to create balance across the various industries and subsequently the world.

3.1.1 The International System (SI) of units

The SI has been recently redefined, based on fundamental constants. Details about the definitions and realization of the SI units is discussed in the [SI Brochure](#), which is published by the BIPM, the intergovernmental organization through which Member States act together on matters related to measurement science and measurement standard⁹.

The seven defining constant of the SI are: ⁹

- The caesium hyperfine frequency $\Delta\nu_{Cs}$;
- The speed of the light in vacuum c ;
- The Plank constant h ;
- The elementary charge e ;
- The Boltzmann constant k ;
- The Avogadro constant N_A ;
- The luminous efficacy of a defined visible radiation K_{cd} .

Now how can we guarantee that the device of the end user is accurate? Accurate measurements are a central component of quality assurance, so the traceability of the measurement become important.

3.1.2 Calibration and Traceability

According to the International Vocabulary of Metrology (VIM), Metrological Traceability or Measurement Traceability is a “property of a measurement result whereby the result can be related to a reference through a documented unbroken chain.” The word “chain” means sequence of measurement standards and calibrations that are used to relate a measurement result to a reference of calibrations where the reference value is the definition of a measurement unit through its practical realization and each contributing to the measurement uncertainty. For comparability of measurement results, the quantities have to be in the same kind, which means are metrologically traceable to the same reference, e.g.

measurement results, for the distances between the Earth and the Moon, and between Paris and London, are metrologically comparable when they are both metrologically traceable to the same measurement unit, for instance, the meter.

From the Figure 3.1 it can be said that the measurement traceability starts from the defined SI units (published by the BIPM). The SI definitions are realized by primary methods, which can be performed by NMIs and Designated Institutes. Because it's neither affordable, efficient or even possible for everybody within a country to work directly with their NMI, NMI-level calibration standards are used to calibrate primary calibration standards or instruments; primary standards are then used to calibrate secondary standards; secondary standards are used to calibrate working standards; and working standards are used to calibrate process instruments. In this way, as illustrated in the image below, references to the SI standards can be efficiently and affordably passed down the calibration pyramid through the NMI, into industry as needed. In this way, working standard used in routine measurements are being calibrated.

By using the calibration value describing the relation to the original reference, the secondary and lower-level standards will also be related to the original reference. At each calibration step, the calibration value is calculated using the calibration data of the reference. Each calibration step generates additional uncertainties that are added to the uncertainty inherited from the previous step. For traceability, this results in a hierarchy with ever increasing uncertainties. This is often represented by a pyramid (Figure 3.1).

Without traceability, a laboratory can claim anything they want in a test or calibration report. With traceability and the independent verification of an accreditation or inspection body, the risk of falling victim to fraudulent information and activities can be minimized. When the equipment is send out for calibration, normally receive a calibration report when the instruments are returned. In these reports are estimates of measurement uncertainty that are associated with the reported measurement results. This

uncertainty will be used in the uncertainty budgets to estimate Calibration and Measurement Capability (CMC) uncertainty published in the scope of accreditation.

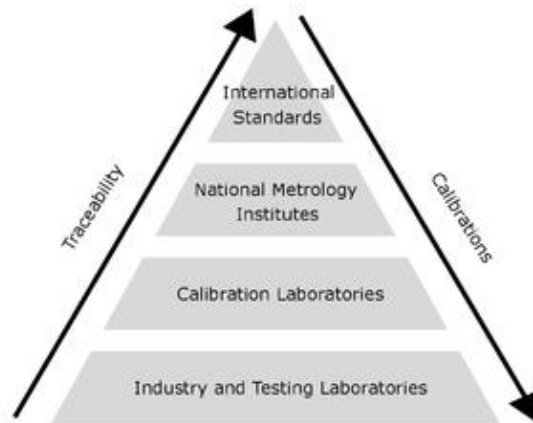


Figure 3.1. Measurement traceability concept and the calibration pyramid.

3.2 Humidity generator

According to the definition of traceability, a standard primary-level system should be in place for humidity measurement device calibration that produces a gas stream with known humidity based on basic and traceable units such as pressure, temperature, and mass. The National Measurement Institute (NMI) uses various humidity generators such as gravimetric hygrometers, two temperature, two flow, two pressure, hybrid, and diffusion methods that operate in different temperature and pressure ranges with certain uncertainties.

Gravimetric hygrometer

In this method, a dry gas of known weight and volume is mixed with water vapor and then the mixture flows into a U-tube containing desiccant and is absorbed by it. There are three U-tubes to increase the accuracy of the absorption process and to ensure that all the gas is absorbed. The absorbed water vapor is weighted. This method is an absolute measurement of humidity because the unit of measurement is the mixing ratio, i.e. the mass of water/mass of dry air is a fundamental quantity. The volume of dry gas

is calculated by the number of times the cylinder is evacuated and filled with known volume. Then, by multiplying the volume by the gas density in the cylinder, the pressure and the temperature, the exact mass of dry air is calculated¹⁰. This system works in the dew/frost point temperature range of -35 °C to 75 °C¹¹.

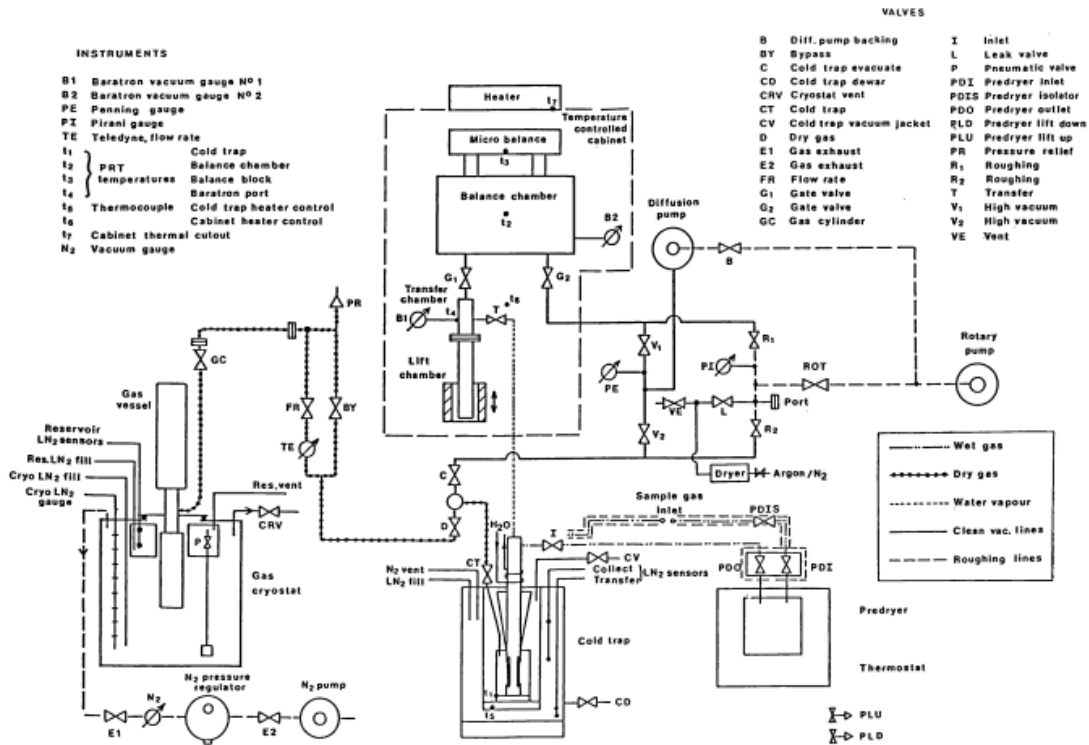


Figure 3.2. Schematic block diagram of a gravimetric hygrometer¹².

Two flows generator

In this method a stream of gas is divided in two flows by using a proportional valve. One part of the gas is saturated over water or ice and the other stream remains dry gas, then they are combined in the test chamber. The two parts are recombined in the test chamber which is filled with water and then exhausted into the room. Water base thermal bath is cheaper than the other low freezing liquid. Moreover, water avoids high temperature gradient in the generator which leads to low uncertainty level. By this technique

at desire temperature a low humidity gas stream is generated. The relative humidity in the test chamber is given by the ratio of the flow division¹³. The mole dilution is:

$$X = \frac{\dot{n}_s x_s + \dot{n}_p x_p}{\dot{N}}$$

where \dot{n}_s, \dot{n}_p are the molar flows of the saturated gas and pure gas, respectively, \dot{N} is the total molar flow, x_s, x_p are the mole fraction of water in the saturated gas and the residual mole fraction of water in the pure gas respectively. The flow range of the generator is between 10 l·min⁻¹ up to 100 l·min⁻¹ and the process pressure is kept constant at 300 kPa¹³.



Figure 3.3. Schematic diagram of a divided flow generator¹³.

Two temperature generator

The principle of this method is to saturate an air stream at lower temperature then to increase the temperature to a higher value at constant pressure $4 \cdot 10^5$ Pa.¹⁴ The generator main parts are four saturators and four test chambers, two liquid baths, four standard platinum resistance thermometers (SPRTs), air compressor. In order to avoid any contamination air was dried and filtered before going to the generator then it was led to pre-cooler heat exchanger comprises six parallel stainless-steel tubes to precondition the air before entering the saturator tube. Saturator temperature sets the dew-point

temperature T_d ¹⁴. In order to have a better contact between the saturator tube and the bath the gas entered again to the copper labyrinthine tube which has high thermal conductivity. This tube is tilted and the air stream is in direct contact with water, then the outlet gas is fully saturated. The generator measuring range covers relative humidity range between 13 % up to 98% with the uncertainty 0.25 % to 0.67 % ($k = 2$)¹⁴.

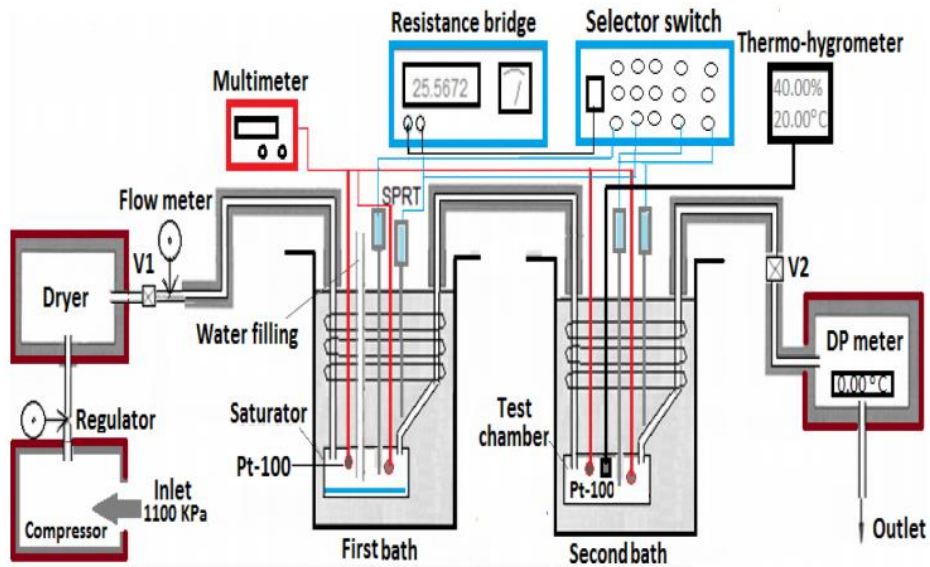


Figure 3.4. Schematic diagram of the two-temperature generator¹⁴.

Two-pressure generator

Two-pressure humidity generator needs a clean, dry and oil free pressurized air which is inside a temperature controlled saturator chamber. The saturator chamber gas temperature T_s and pressure P_s are measured then the gas is expanded through an isothermal valve to the ambient pressure. Then conducted to the test chamber and again its temperature and pressure (T_c, P_c) is measured¹⁵. This method is one of the most used because at a constant temperature by varying the pressure a wide range of the humidity can be generated and also it so fast because changing the pressure is easier than temperature variation. According to the Dalton's law, at constant temperature, the gas mixture pressure is the sum of

each partial pressures if it occupies the volume at the same temperature, so the relative humidity is measured by the following equation¹⁵:

$$RH \% = \frac{f(P_s, T_s)}{f(P_c, T_c)} \frac{e_w(T_s)}{e_w(T_c)} \frac{P_c}{P_s} \cdot 100 \%,$$

$$f(P_s, T_s) = \frac{x_w P_s}{e_w(T_s)} = \frac{(1 - x_g) P_s}{e_w(T_s)},$$

$$f(P_c, T_c) e_w(T_d) = f(P_s, T_s) e_w(T_s) \frac{P_c}{P_s}$$

where $f(P_s, T_s)$ is the enhancement factor of the saturated gas, $f(P_c, T_c)$ is the enhancement factor of the test chamber, x_g, x_w are the mole fraction of the gas and water vapor, $e_w(T_d)$ is the saturation vapor pressure at the thermodynamic dew point.

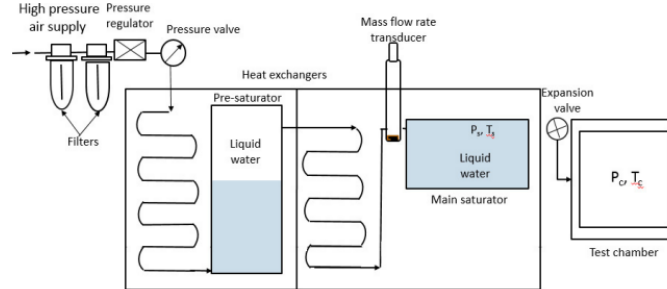


Figure 3.5. Schematic diagram of two-pressure humidity generator. ¹⁵

Hybrid method

For calibration in the frost point temperature between -70 °C and $+85$ °C, a mole fraction of $1 \cdot 10^{-6}$ mol mol⁻¹ to 0.56 mol mol⁻¹ and a gas flow of up to 150 l·min⁻¹ by coupling two-pressure and split flow, the hybrid humidity generator (HHG) was developed¹³. In this method, the gas is saturated using a pre-saturator and to ensure complete saturation with minimum uncertainty, there is a final saturator consisting of a heat exchanger over a saturation chamber that is stable within 1 mK¹³; the stability of the saturation chamber minimises the latent heat lost by the incoming gas. When a gas with a higher dew point than that of the saturation chamber flows through the chamber, the additional water vapour

condenses out and flows back into the chamber¹³. The mole fraction X of water vapor in the gas is then calculated using the equation:

$$X = \frac{e(T_s)}{P_s} * f(T_s, P_s)$$

where T_s and P_s are the temperature and pressure of the gas and water in the saturator, $e_w(T_s)$ is the water-vapor pressure at T_s . The enhancement factor $f(T_s, P_s)$ reflects departures from ideal solution behavior and non-ideal gas effects.

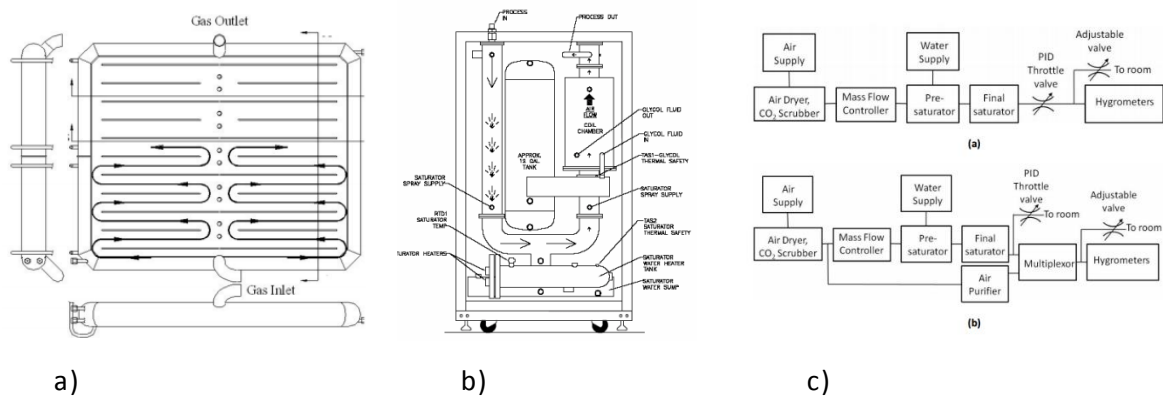


Figure 3.6. Schematic diagram of the hybrid saturator. The overall view of the saturator (a), the pre-saturator (b), the schematic diagram of a two-pressure mode(c.a), and the divided flow (c.b)¹³.

Diffusion tube generator

The principle of this method is based on molecular diffusion, which is estimated by Fick's law. The generator consists of a purifier that dries the incoming nitrogen (N_2) and is connected to the thermal mass flow controller so that part of the dry gas reaches the inlet of the generator, which consists of a stainless steel chamber, and the rest of the flow is bypassed¹⁶. The inner surfaces of the tubes and the chamber were electrochemically polished. To create a closed system, the test chamber is connected to a magnetic levitation balance (MSB) via a vacuum flange. At the inlet of the test chamber, the incoming dry N_2 gas is diluted by the water vapour from the diffusion cell. The wet outlet gas was again mixed with the diverted flow. The temperature of the test chamber is measured with a platinum resistance thermometer (PRT)

attached to the chamber. Another PRT is used to measure the internal temperature of the test chamber. This temperature difference is important for estimating the diffusion water temperature. The working temperature range for the chamber test is between 25 °C and 55 °C. A pressure regulator was used to control the absolute pressure in the chamber at 150 kPa and 450 kPa. An analytical balance with a readability of 1 µg and an MSB coupled by a permanent magnetic non-contact suspension coupler (MSC) is used to balance the cycle. By applying a constant voltage and the position sensors, the electromagnet is controlled in a vertical position the diffusion tube so that the diffusion and evaporation rate is adjusted. There is a software program that controls the MSB and data acquisition. There is also a CRDS to monitor the water vapour mole fraction¹⁶.

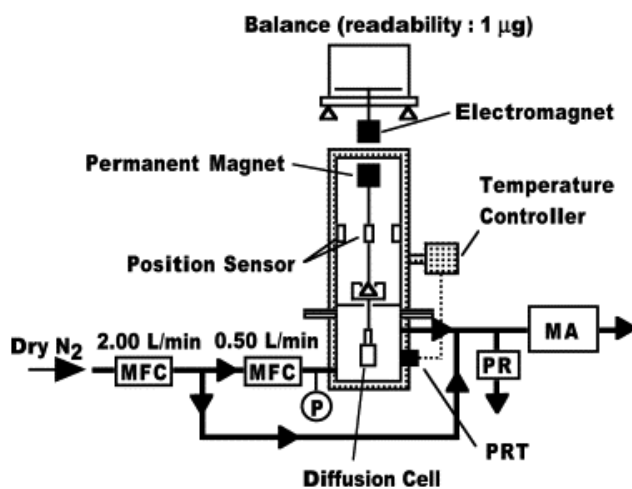


Figure 3.7. Schematic of the diffuse-tube¹⁶.

4. A novel humidity standard

4.1 Introduction

The analysis of water vapour impurity is important in a number of the cutting-edge technology, fields such as the semiconductor manufacturing process, display industry, and gas industry. The sensing of trace-moisture in gases, with an amount-of substance fraction less than $1 \mu\text{mol}\cdot\text{mol}^{-1}$, has become increasingly important in the recent decade, because it has been recognized that even such a small amount of water vapour plays a critical role in the yield and product quality.

With increasing frequency in the sciences and in industrial and technological areas measurements of trace quantities of water vapour are being made. For example, in 1900s, with the emerge of modern astrophysics, the measurement of the moisture content of planetary atmospheres, particularly that of Mars, continues to challenge astronomers and space scientists. Processes in the chemical industry, such as butane isomerization, are affected by very low levels of humidity. In semiconductor manufacturing, very small quantities (100 ppb) of water vapour can adversely affect the performance and the yield of silicon-based semiconductors, the ratio between the number of silicon wafers batches that can be sold and the number of silicon wafers batches that can be made. Reliable measurements are ensured by means of calibrated sensors and instruments. To fulfil this need, in 1973, the National Institute of Standards and Technology (NIST) developed and put into operation a two temperature Low Frost Point Generator (LFPG). This calibration facility was designed in order to calibrate over the range frost points from $-30\text{ }^{\circ}\text{C}$ to $-100\text{ }^{\circ}\text{C}$, at pressures range from 500 to 200000 Pa.¹⁷ The dry gas was moisturized with the evaporated and saturated water vapour rising from the ice surface. The saturator residing within an evacuated enclosure, a flow control for carrier gas, temperature and pressure measuring instrumentation were used. In order to maintain the saturator temperature stability a multimode closed comprising Peltier heat-pump closed loop temperature control scheme comprising Peltier heat-pump thermoelectric devices and a mechanical

refrigeration system were installed. The expanded ($k = 2$) relative uncertainty of the produced mole fraction of water vapour in air was less than 0.8 %, while for humidity expressed in terms of frost-point temperature the expanded uncertainty was 0.013 °C. ¹⁷

At the D.I.Mendeleev Institute for Metrology (VNIIM) in Russia a humid gas generator in trace was developed, based on the same phase equilibrium principle. The generator consisted in direct reproduction of the humid gas saturation state over a plane condensed layer of ice at a given temperature, which represents the frost point temperature. The system consisted of a pre-saturator and a main saturator set in a thermal insulated temperature-controlled chamber. Evaporated liquid nitrogen was used as a coolant in the chamber and the temperature inside the chamber was maintained equal to the required frost-point temperature. The generator was able to work between -100 °C and $+20$ °C with the uncertainty of 0.1 °C at 95 % confidence level ($k = 2$). ¹⁸ In 2006, a low frost-point humidity generator was realised at the Korea Research Institute of Standards and Science (KRISS). The control range of the for frost-point temperature, that was between -99 °C and -40 °C corresponding in terms of water vapour mole fraction to the range from $18 \text{ nmol} \cdot \text{mol}^{-1}$ to $130 \text{ } \mu\text{mol} \cdot \text{mol}^{-1}$, was provided by means of a two-stage compression refrigerator provided with thermoelectric devices. The obtained standard uncertainty on the generated frost point temperature was less than 32 mK between -70 °C to -40 °C and increased to 137 mK at -90 °C. ¹⁹ Since 2006, in order to extend the calibration capability down to a frost-point temperature of -105 °C ($4 \text{ nmol} \cdot \text{mol}^{-1}$), a two-temperature, two-pressure generator type is used. When the frost-point temperature is -105 °C, the combined ($k=2$) expanded uncertainty in the generated humidity raises to 0.72 °C ($0.8 \text{ nmol} \cdot \text{mol}^{-1}$). ²⁰ In the new NIST generator, the LFPG operating range (*ppb*) is extended to *ppt* levels by diluting the water vapor/gas mixture produced by the LFPG in NIST. ²¹

At the Italian National Institute of Research in Metrology (INRIM), a new saturation based one-temperature one-pressure, 1T1P, low-frost point primary generator able to operate at sub-atmospheric pressure has been designed and constructed. The generator consists of a thermostatic bath which sets

the frost point temperature within the range of $-99\text{ }^{\circ}\text{C}$ and $-20\text{ }^{\circ}\text{C}$. The saturator is immersed in the thermostatic bath and the inlet gas by passing through isothermal ice becomes fully saturated. The generator can work in the pressure range between 1100 hPa and 200 hPa. ²²

4.2 Design of a trace water generator

A schematic of the trace water generator realized at INRIM is shown in Figure 4.1. ²² Figure 4.1(a) shows the stainless steel 316 L saturator, which is made of 11 coils with external radius of 60 mm and an internal radius of 40 mm plus an outlet plenum, where water in excess is collected. The total height is of 166 mm. The passageway (Figure 4.1(b)), of which about 40 % is filled up with ice and the remaining 60 % is left empty for the gas passage, has a cross section of 14 mm in width and 9 mm in height. The vertical connection holes of 8 mm in diameter let the gas to flow from one coil to the following one.

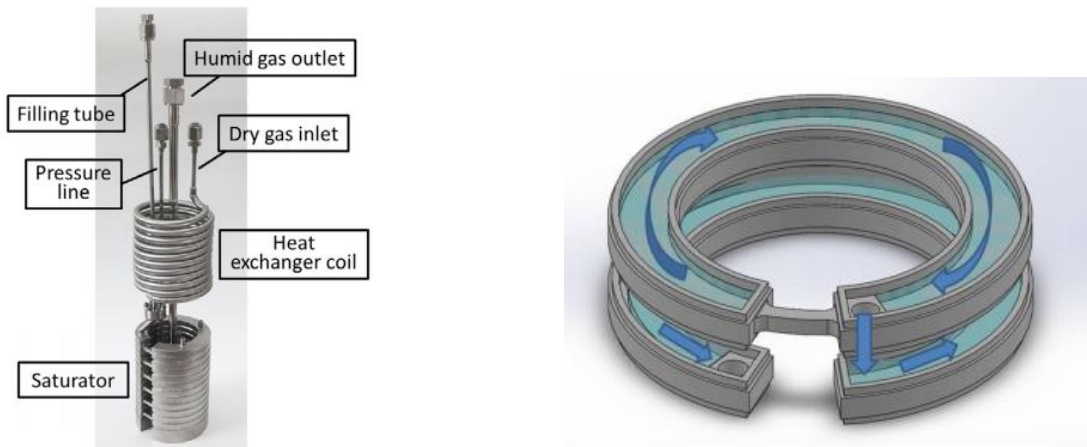


Figure 4.1. (a) Schematic diagram of the low frost-point generator, heat exchanger and the saturator where the inlet gas is conditioned. (b) Cross section of the saturator passage. ²²

The thermostatic bath, which allows maintaining a constant temperature between $-99\text{ }^{\circ}\text{C}$ and $-20\text{ }^{\circ}\text{C}$, contains the saturator and the heat exchanger. The saturated gas temperature T_{sat} which corresponds to the generated frost-point temperature, is measured by a capsulated glass $25\ \Omega$ standard platinum

resistance thermometer (SPRT) (see figure 4.2) in thermal equilibrium with the saturated humid gas flow. At the same depth inside the bath there is a secondary platinum resistance thermometer (PRT) to measure the temperature of the saturator T_{bath} . The precise thermometer bridge collects thermometers temperatures. A PID controller, which sets the opening of an electro-valve toward the vacuum pump, and a back pressure control, based on a pressure transducer to measure the saturator pressure, keep the saturator pressure at a constant value between 200 hPa and 1100 hPa. With a full scale of $10 \text{ l}\cdot\text{min}^{-1}$ mass flow controller, the flow rate \emptyset of the inlet gas is controlled. The generator is a one way saturator where only 60 % of the passage are free and the rest is filled by an isothermal ice. If the inlet gas frost point temperature is higher than the T_{bath} , the generator will work as a condenser. In order to prevent ice formation in the heat exchanger, with a consequent block of the gas passage, before the generator inlet there is a drying system, consisting of a purifier and a molecular sieve in series in order to further reduce the frost-point temperature of the nitrogen below the T_{bath} .²²

Water vapour mole fraction of the saturated gas is measured by a cavity ring down spectroscopy analyser (CRDS). The CRDS is working in the pressure range between 80 hPa and 2650 hPa, while the pressure and flow rate inside the CRDS is regulated at 100 Torr ($\sim 133 \text{ hPa}$). To assure at least a flow rate of about $0.5 \text{ l}\cdot\text{min}^{-1}$ through the instrument, the outlet of the spectroscopy analyser is connected to a vacuum pump. The connection pipe between the saturator outlet and the CRDS inlet is placed in the ambient air. To avoid the risk of ice formation on its outside wall due to ambient air humidity condensation, the tube is insulated and heated at $40 \text{ }^\circ\text{C}$.²²

Schematic diagram of the whole system is shown in Figure 4.2.²²

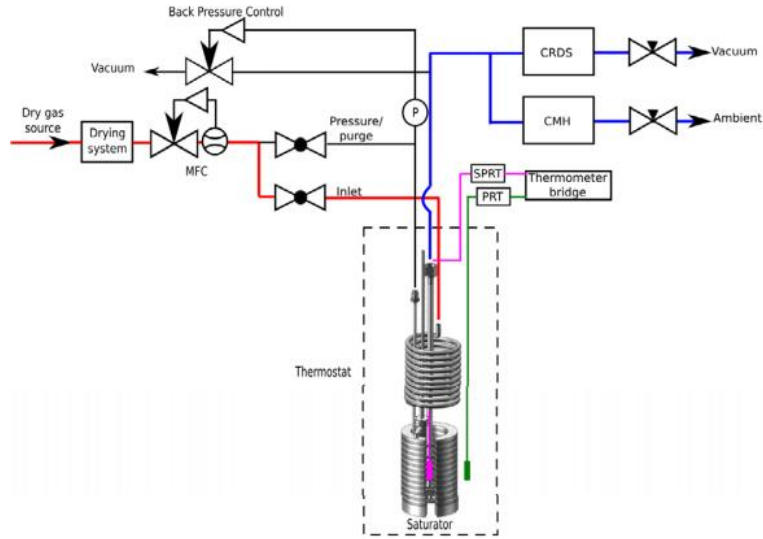


Figure 4.2. Schematic diagram of the experimental apparatus: the generator, the humidity sensors chilled mirror hygrometer (CMH) and the cavity ring down spectroscopy (CRDS).²²

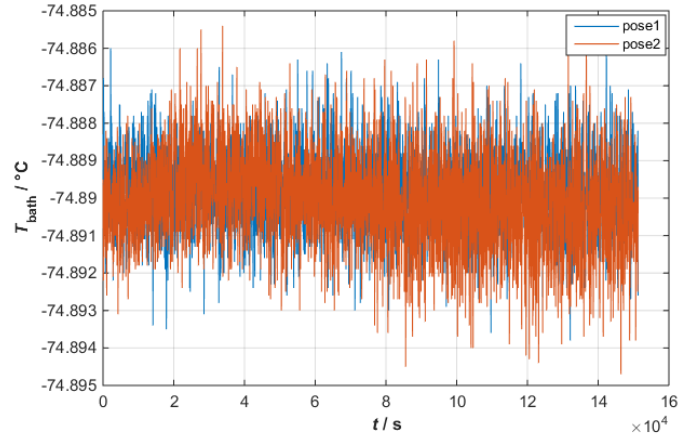
4.3 Experimental evaluation of the generator performance

According to Chapter 2, water vapour mole fraction can be expressed as a function of the temperature, T , pressure, P , and the non-ideality of the gas, f , as given by Eq. (1).

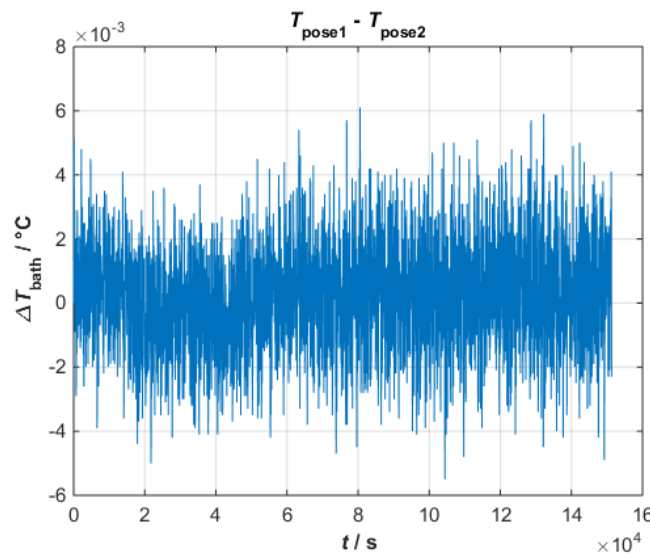
$$x_w = \frac{e_w(T)f(T, P)}{P} \quad (1)$$

The temperature stability of the saturator is a very important factor in the performance of the generator. The stability of the thermal bath temperature influences the temperature of the saturator, T_{bath} , thus the saturated gas temperature, T_{sat} . A uniform temperature of the bath means a uniform temperature of the saturator, which is investigated by measuring T_{bath} in two different positions. The PRT is moved from position two (pose 2), which corresponds to the saturated gas outlet, to position one (pose 1) which is about 10 cm above position two and in correspondence of the SPRT (Figure 4.2). In Figure 4.3 an example of the uniformity of the saturator temperature determined at $T = -75 \text{ }^\circ\text{C}$ and $P = 1100 \text{ hPa}$ is shown. Further

measurements carried out in the temperature range between $-99\text{ }^{\circ}\text{C}$ and $-80\text{ }^{\circ}\text{C}$ at $P = 1100\text{ hPa}$ are reported in Appendix.



a)

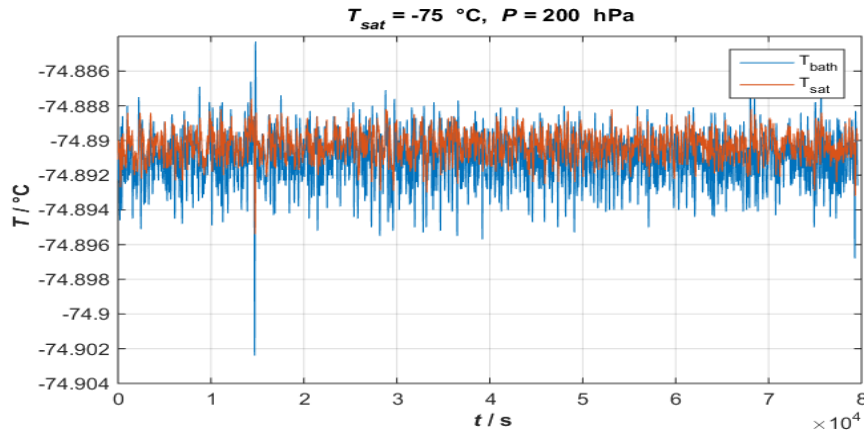


b)

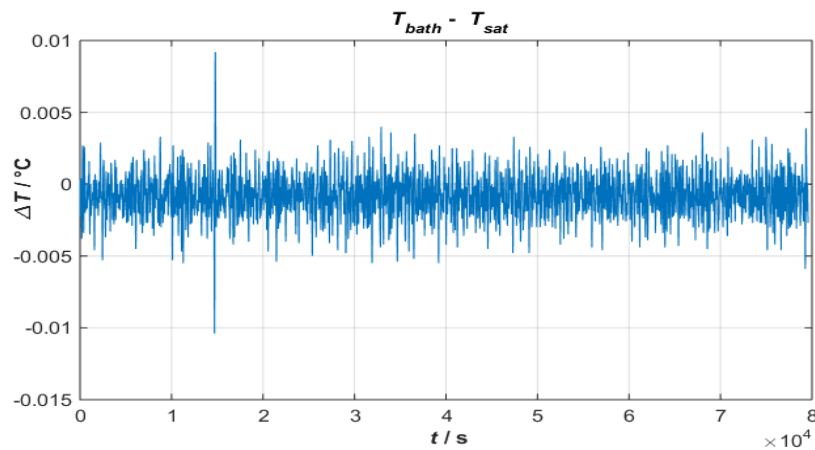
Figure 4.3. a) Measurement of the saturator temperature at two different depths as a function of the time for a nominal $T_{\text{sat}} = -75\text{ }^{\circ}\text{C}$ and $P = 1100\text{ hPa}$. The red line represents pose 1 temperature, the blue one is the saturator temperature at pose 2; b) Uniformity of the saturator temperature, ΔT , as a function of the time. It is determined by the difference between the two temperatures.

Variations in T_{bath} along the saturator results to be less than $0.005\text{ }^{\circ}\text{C}$, thus the uniformity of the saturator is better than $0.005\text{ }^{\circ}\text{C}$. The agreement between T_{sat} and T_{bath} is also investigated. Indeed, the measurement of the temperature uniformity of the saturator by means of the PRT placed in the liquid

bath has sense only if T_{sat} and T_{bath} are consistent. The SPRT in the outlet tube can't be moved; in its placed the PRT is shifted along the vertical axes of the saturator.



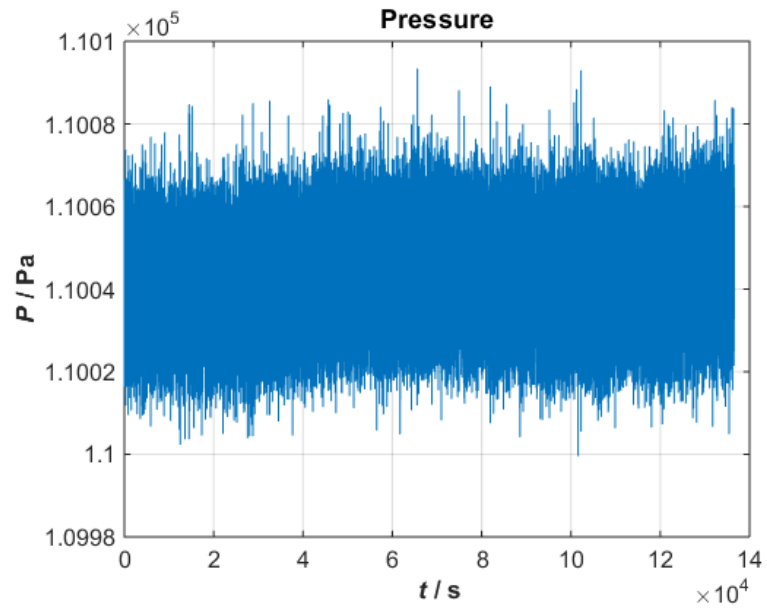
a)



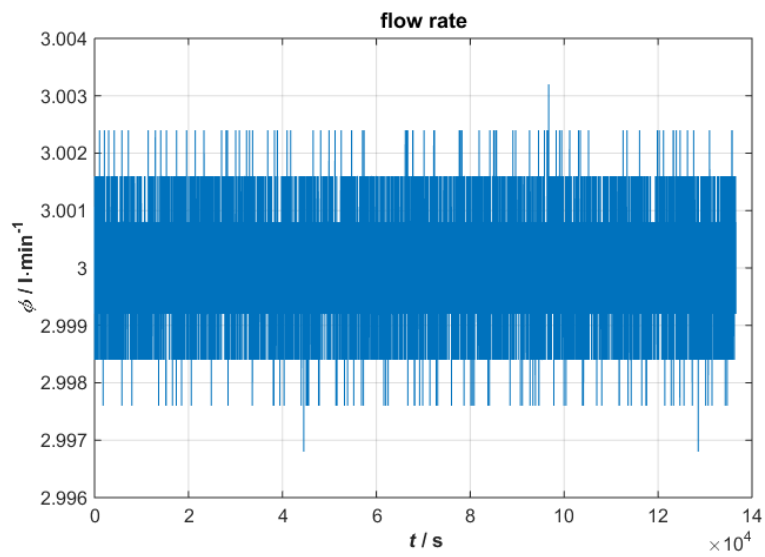
b)

Figure 4.4. a) Saturator temperature, T_{bath} , (blue line) and saturated gas temperature, T_{sat} , (red line) measured by the PRT in pose 1 and the SPRT, respectively. Nominal measurement conditions: $T = -75 \text{ }^\circ\text{C}$, $P = 200 \text{ hPa}$. b) Correspondent difference between T_{bath} and T_{sat} as a function of the time.

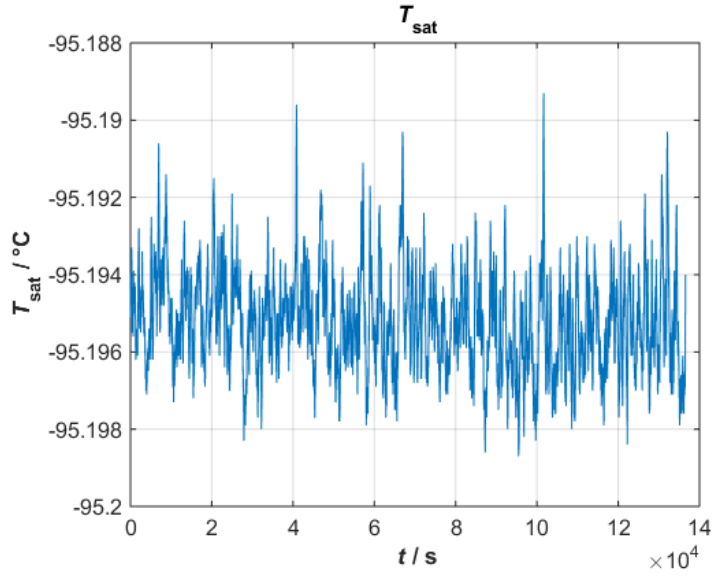
In order to evaluate the performance of a 1T1P generator the assessment of the flow-rate, temperature and pressure stability is important. Stability of saturator and bath temperature, pressure and flow rate is shown in figure 4.5 where T_{sat} is nominally $-95 \text{ }^\circ\text{C}$, $P = 1100 \text{ hPa}$ and the gas flow-rate ϕ is $3 \text{ l}\cdot\text{min}^{-1}$.



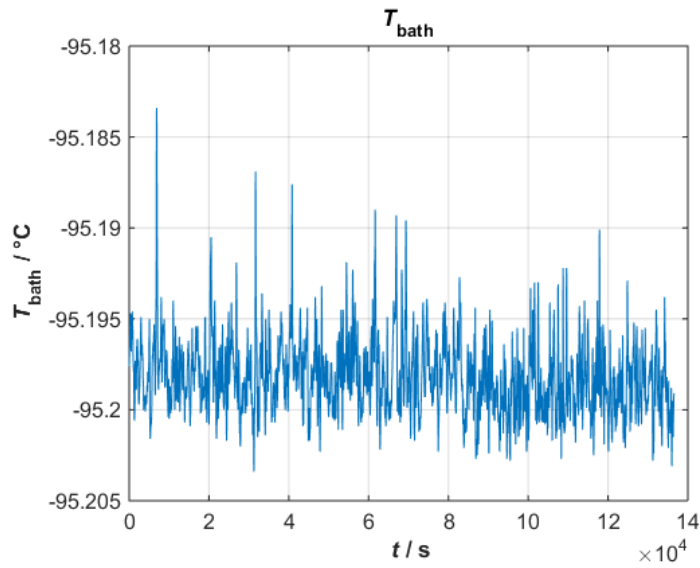
a)



b)



c)

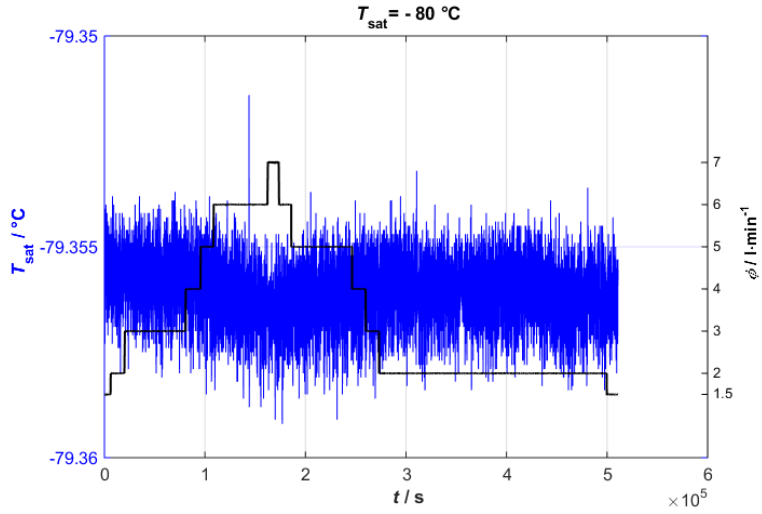


d)

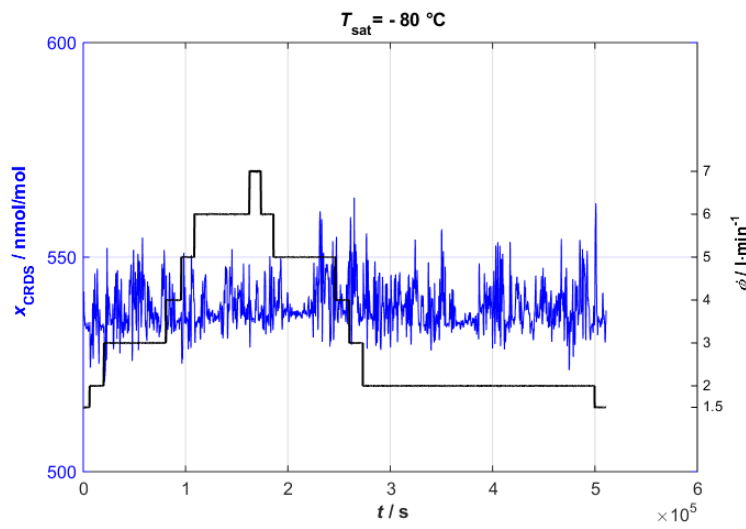
Figure 4.5. Experimental condition at $T_{\text{sat}} = -95 \text{ }^\circ\text{C}$, $P = 1100 \text{ hPa}$, $\varphi = 3 \text{ l}\cdot\text{min}^{-1}$. Variation of pressure (a), flow rate (b), saturated gas temperature measured by SPRT (c), and saturator temperature measured by PRT (d).

As depicted in Figure 4.5(a) the pressure standard deviation is 15 Pa, in Figure 4.5(b) the flow-rate standard deviation is $0.002 \text{ l}\cdot\text{min}^{-1}$ and in Figure 4.5 (c, d) the temperature of the saturated gas and of the saturator have a standard deviation of $0.001 \text{ }^\circ\text{C}$.

Another aspect that need to be investigated to evaluate the performance of the generator is its efficiency. The efficiency of the saturator is evaluated by monitoring the outlet gas frost point temperature T_{fp} , or the equivalent water vapour mole fraction as flow rate of the inlet gas is varied. Inlet gas needs an adequate path length to be in contact with the isothermal ice to reach fully saturation condition. The saturator has a constant length, thus to vary the flow rate means to vary the contact time with the ice. In this thesis work, the saturator efficiency has been evaluated by measuring variations in x_w as a function of the flow rate, ϕ , at different values of T_{sat} and P . The carrier gas flow rate at the inlet of the generator was varied between $1.5 \text{ l}\cdot\text{min}^{-1}$ and $7 \text{ l}\cdot\text{min}^{-1}$. In Figure 4.6 the temperature of the generated gas which is supposed to be fully saturated, T_{sat} , and the water vapour mole fraction measured by the CRDS analyser are reported as an example for a T_{sat} of about $-80 \text{ }^\circ\text{C}$ and pressure 1100 hPa, while the flow rate is varying. The efficiency of the generator is evaluated determining the difference between the saturated gas temperature and the equivalent frost-point temperature of the water vapour mole fraction measured by the CRDS at different values, using as a reference the difference between T_{sat} and T_{fp_CRDS} measured at $1.5 \text{ l}\cdot\text{min}^{-1}$, thus assuming that at the lower flow rate the gas is completely saturated. In Figure 4.7 the efficiency results obtained at $T_{sat} = -90 \text{ }^\circ\text{C}$ and $T_{sat} = -95 \text{ }^\circ\text{C}$ are reported with the corresponding uncertainties. In both cases the generator behaviour for different flow rate is consistent within the uncertainties and the overall performance of the system results independent from the flow rate.



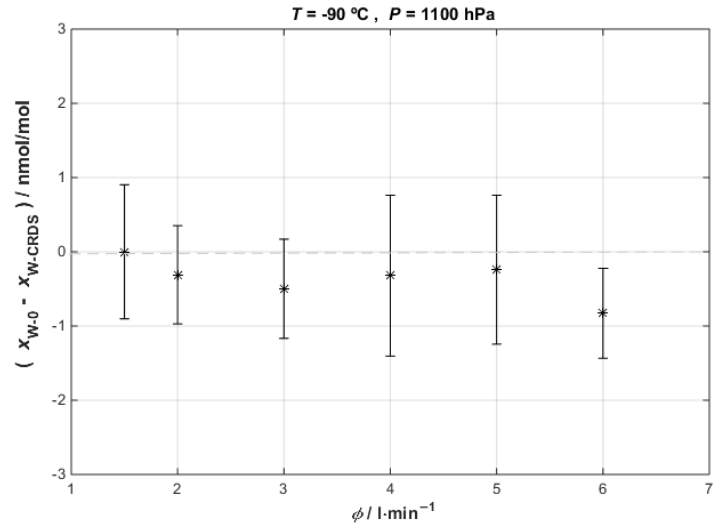
a)



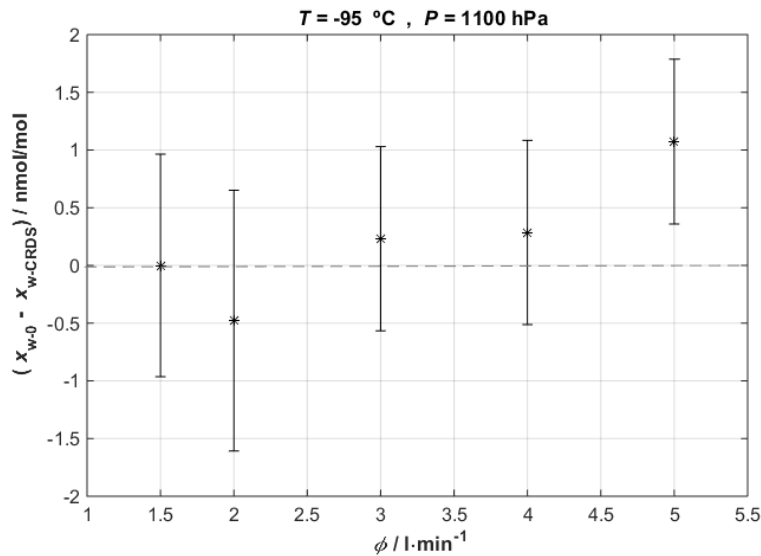
b)

Figure 4.6. a) Saturated gas temperature measured by the SPRT as a function of the time at $P = 1100$ hPa. b)

Respective water vapour mole fraction measured by the CRDS. The red line makes reference to the flow rate.



a)

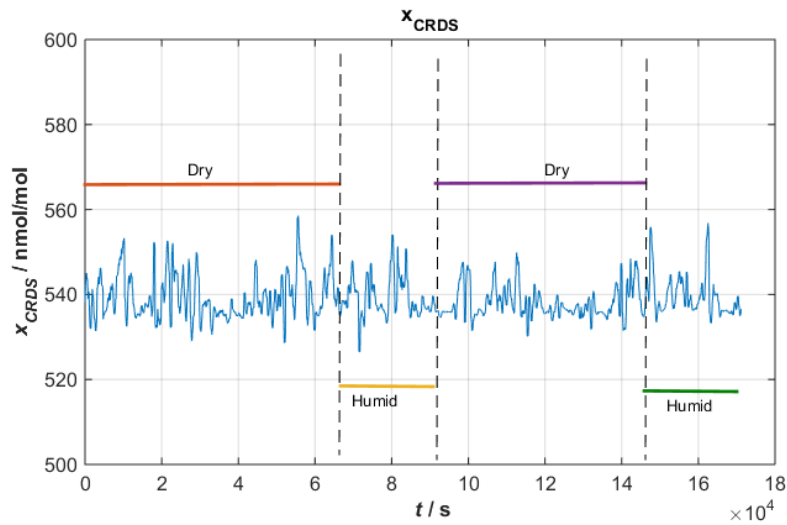


b)

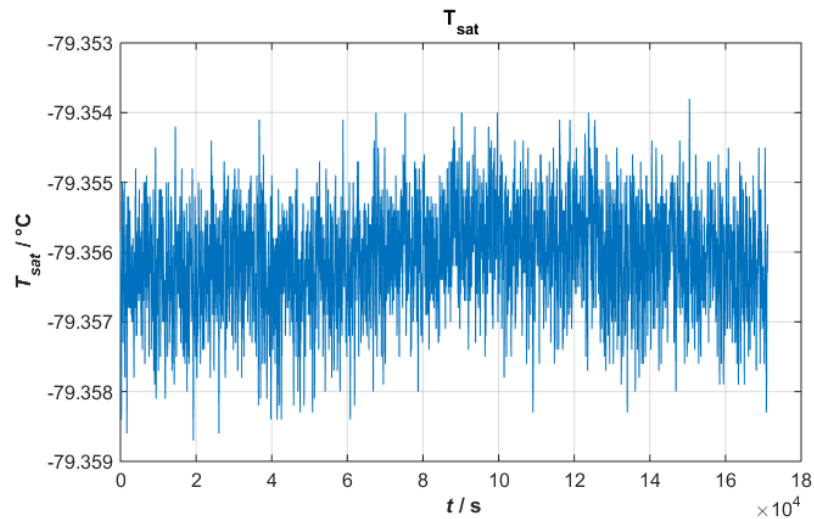
Figure 4.7. Difference between water vapour mole fraction generated, $x_{w,0}$, and the reading of CRDS, x_{w-CRDS} , for different flow rate at $P = 1100\text{ hPa}$ and $T_{\text{sat}} = -90\text{ }^{\circ}\text{C}$ (a) and $T_{\text{sat}} = -95\text{ }^{\circ}\text{C}$ (b).

Actually the saturation capability of the generator was also investigated by alternating a dry gas and a humid gas at the inlet of the system. Generally, in order to prevent ice formation in the heat exchanger, a series of sieves are used at the inlet of the system in such a way the inlet gas frost point temperature is less than $-99\text{ }^{\circ}\text{C}$ (lower limit of the generator working range) and is conditioned through the passage in the saturator. But if the inlet gas frost point temperature is higher than the generator frost point, the

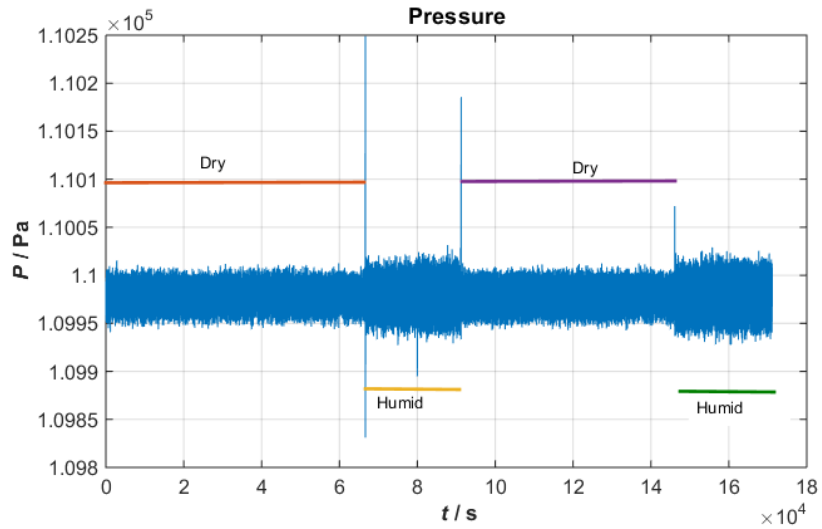
generator will work as a condenser. The inlet gas frost point is measured directly by a chilled mirror hygrometer and it is known, $-75\text{ }^{\circ}\text{C}$, while the generator temperature is set at $-80\text{ }^{\circ}\text{C}$, $-85\text{ }^{\circ}\text{C}$, $-90\text{ }^{\circ}\text{C}$. In Figure 4.8 are reported the results of the experiment carried out at $T_{\text{sat}} = -80\text{ }^{\circ}\text{C}$. The other plots can be found in the Appendix.



a)



b)

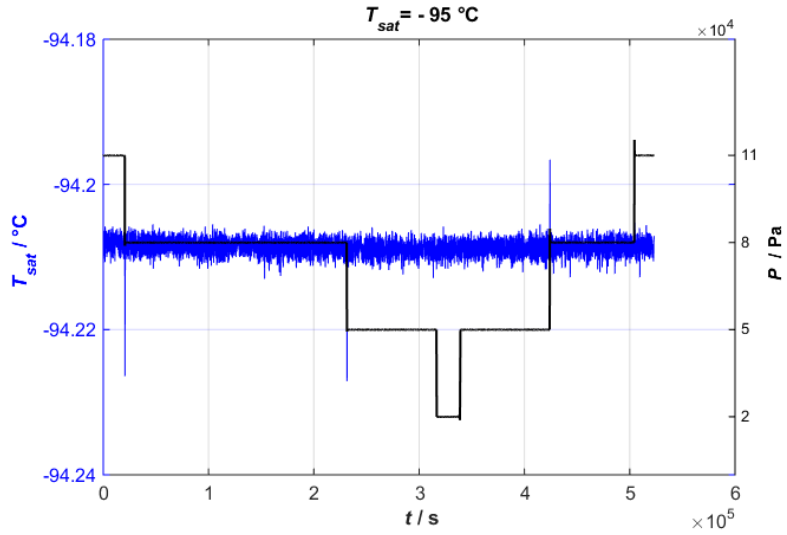


c)

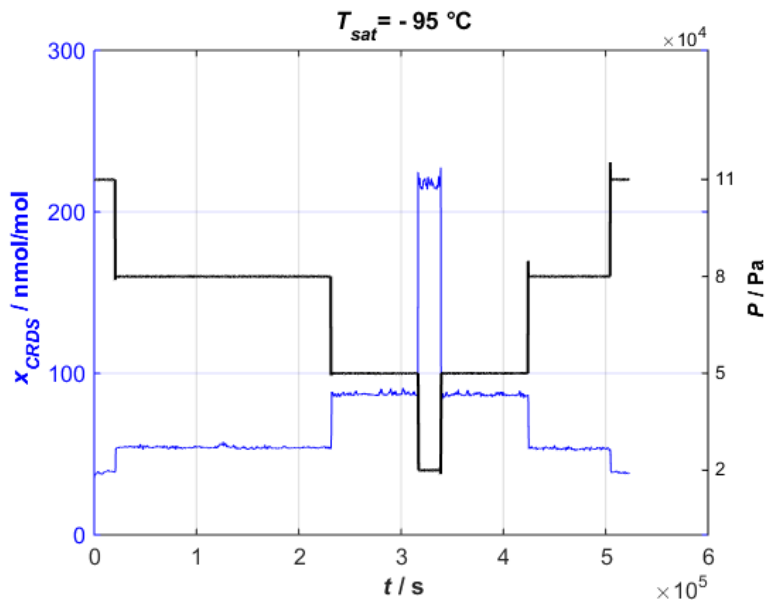
Figure 4.8. Variation of the water vapour mole fraction measured by CRDS (a), of the saturated gas temperature measure by SPRT(b) , and pressure stability by varying the inlet gas from humid to dry(c)

As depicted the standard deviation for T_{sat} in both dry and humid is 0.001 °C, the dry gas pressure standard deviation is 16 Pa, while the humid gas standard deviation is 22 Pa. The standard deviation of the CRDS reading for the dry gas is 5 ppb whereas for the humid gas standard deviation is 4 ppb. So as a result, the generator can work in a proper way and independently of the inlet gas condition and still be stable.

The reproducibility capability of the system is checked by changing the flow rate or the pressure of the system. In figure 4.9 the result of the experiment for the frost point temperature at -95 °C at different pressure is reported. The standard deviation of the pressure is 100 Pa, for the saturated gas temperature, regardless of the bath temperature, the standard deviation is 0.010 °C and for the measured water vapor mole fraction is 5 ppb.



a)



b)

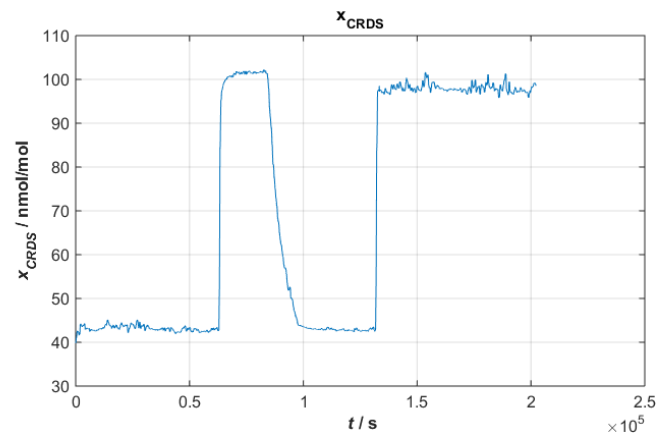
Figure 4.9. Variation of the saturated gas temperature (a-blue line) and of the water vapour mole fraction (b-blue line) by changing the pressure (200 hPa, 500 hPa, 800 hPa, and 1100 hPa).

In all the experiment the T_{sat} standard deviation is less than $0.001\text{ }^{\circ}\text{C}$, the flow rate standard deviation is $0.002\text{ l}\cdot\text{min}^{-1}$, the pressure standard deviation is 13 Pa , and the water vapour mole fraction standard deviation is 5 ppb . So all the standard deviation is in the uncertainty range.

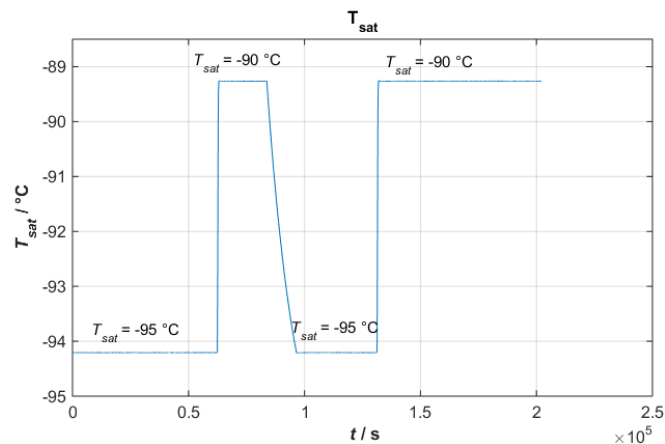
To evaluate the repeatability of the measurements, the saturated gas temperature was changed by step of 5 °C from -95 °C to -90 °C and backwards. Repeatability means the dispersion of the results when the experiment is carried out in the same conditions, in other words with the same measurement process, observer, instrument location and operating conditions.

The obtained results are reported in Figure 4.10, where the behaviour of the water vapour mole fraction is shown as a function of the time (a) in correspondence of the saturated gas temperature T_{sat} profile (b).

The test is performed keeping the total gas pressure and the flow rate of the inlet gas constant. The standard deviation of the pressure is 15 Pa and the flow rate fluctuation is less than 0.002 l·min⁻¹.



a)



b)

Figure 4.10. Experimental result of the saturated gas when $P = 1100$ hPa and $\Phi = 3$ l·min⁻¹. a) Water vapour mole fraction reading by the CRDS. b) Saturated gas temperature measured by SPRT when the T_{sat} is varying between -90 °C and -95 °C.

5. Uncertainty evaluation

5.1 Introduction

When reporting the result of a measurement of a physical quantity, it is obligatory that some quantitative indications of the quality of the result be given, so that an interval of reasonable values can be assigned to the measurand. Without such an indication, measurement results cannot be compared, either among themselves or with reference values given in a specification or standard. It is therefore necessary that there be a readily implemented, easily understood, and generally accepted procedure for characterizing the quality of a result of a measurement.²³

According to the International vocabulary of metrology (VIM),²³ a measurement result is “a set of quantity values being attributed to a measurand together with any other available relevant information. A measurement result is generally expressed as a single measured quantity value and a measurement uncertainty. The measurement uncertainty is a non-negative parameter characterizing the dispersion of the quantity values being attributed to a measurand, based on the information used”. Thus the uncertainty is a quantification of the doubt about how well the measurement result represents the value of the measurand.

In a measurement there are several possible sources of uncertainty such as an incomplete definition of the measurand, an imperfect realisation of the definition of the measurand or inadequate knowledge of the effects of environmental conditions on the measurement or imperfect measurement of environmental conditions. Other sources of uncertainty can be e.g. a personal bias in reading analogue instruments, a finite instrument resolution or discrimination threshold, inexact values of measurement standards and reference materials and variations in repeated observations of the measurand under apparently identical conditions.

In most cases, a measurand, denoted by Y , is not measured directly, but is determined from N other quantities denoted by $X_1, X_2, X_3, \dots, X_N$ through a functional relationship f :

$$Y = f(X_1, \dots, X_N) \quad (1)$$

Therefore, the estimate y of Y is given by:

$$y = f(x_1, \dots, x_N) \quad (2)$$

where x_1, \dots, x_N are the estimates of the input quantities X_1, \dots, X_N .

The standard deviation of the estimate y , termed combined standard uncertainty, $u_c(y)$, is then obtained by combining the standard deviation of the input estimates $x_1, x_2, x_3, \dots, x_N$ denoted by $u(x_i)$ as follows:

$$u_c(y) = \sqrt{\sum_{i=1}^N \left(\frac{\partial f}{\partial x_i}\right)^2 u^2(x_i)} \quad (3)$$

where $\frac{\partial f}{\partial x_i}$ are the sensitivity coefficients, that describe how the estimate y varies with changes in the values of the input estimates x_i and $u(x_i)$ is the standard uncertainty (defined as standard deviation) associated with the estimate x_i .

If the input quantities $X_1, X_2, X_3, \dots, X_N$ are not independent, correlations coefficients need to be considered in Eq. (4).

$$u_c(y) = \sqrt{\sum_{i=1}^N \left(\frac{\partial f}{\partial x_i}\right)^2 u^2(x_i) + 2 \sum_{i=1}^{N-1} \sum_{j=i+1}^N \frac{\partial f}{\partial x_i} \frac{\partial f}{\partial x_j} u(x_i, x_j)} \quad (4)$$

The estimates x_i and their standard uncertainties $u(x_i)$ are determined, in turn, by considering the distribution of possible values of the quantities X_i .

If the probability distribution of the values is based on a series of observations of X_i (frequency based), an evaluation of Type A of the standard uncertainty components is carried out, otherwise, a Type B evaluation is applied founded on a priori distribution of the values of X_i .

In the case of a Type A evaluation of standard uncertainty, the estimate x_i can be determined as the arithmetic mean or average of n independent observations as follows:

$$x_i = \overline{X_i} = \frac{1}{n} \sum_{k=1}^n X_{i,k} \quad (5)$$

While the standard uncertainty $u(x_i)$ is given by the experimental standard deviation $s(\overline{X_i})$ calculated as:

$$u(x_i) = s(\overline{X_i}) = \sqrt{\frac{1}{n \cdot (n-1)} \sum_{k=1}^n (X_{i,k} - \overline{X_i})^2} \quad (6)$$

If the estimate x_i of the quantity X_i is not obtained from repeated observations, its standard uncertainty $u(x_i)$ is estimated using a Type B evaluation, that is an evaluation based on the available information on the variability of X_i . This kind of information includes e.g. past experience of the measurements, data from calibration certificates and manufacturer's specifications. The uncertainty in the calibration certificate is usually expressed as an expanded uncertainty. According to the Guide to the Expression of Uncertainty in Measurement (GUM)²⁰, in order to provide an interval within which a wider fraction of the measurements results encompassed, the expanded uncertainty is used. The fraction depends on the coverage factor, k , or level of confidence of the measurement probability distribution function. So the expanded uncertainty, $U(y)$, is the multiple of the combined uncertainty depending on the coverage factor.

For example if measurement result set in the normal probability distribution function (Gaussian distribution) by simply calculating the mean and standard deviation 68% of the statistical data will be in

one standard deviation of the mean, 95 % will lie in two standard deviation of the mean, and 99.7 % will set in three standard deviation of the mean (figure 5.1).

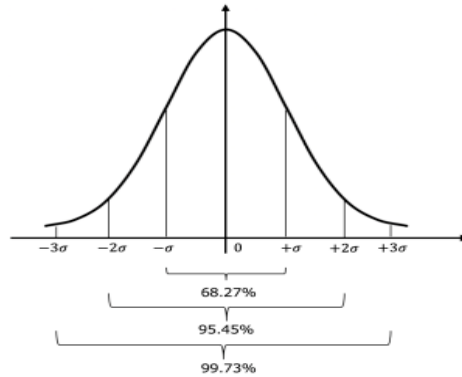


Figure 5.1. Normal probability distribution and confidence levels, $k = 1$ (68 %), $k = 2$ (95 %), $k = 3$ (99.7 %).

5.2 Uncertainty analysis of the trace water generator

In this paragraph the evaluation of the uncertainty budget for the generated frost point temperature T_{fp} , and the corresponding water vapour mole fraction, x_w , is shown. The evaluation is carried out in the temperature working range between -75 °C and -99 °C and in the pressure range from 200 hPa up to atmospheric pressure.

The sources of uncertainty taken into account for the estimate of the uncertainty of the frost point temperature, $u(T_{fp})$, are listed in Table 5.5, 5.6, 5.7 and 5.8. Some of them have been evaluated as Type B uncertainty, while others have been evaluated as Type A.

More in details, among the considered components for the estimate of $u(T_{fp})$, a Type B evaluation has been applied to the following contribution:

SPRT CALIBRATION - The uncertainty contribution is provided by the calibration certificate in terms of extended uncertainty ($k = 2$). Here the standard uncertainty has been evaluated taking into account the

reproducibility of the temperature at the fixed points of the ITS-90. For this reason the probability distribution function considered is the Gaussian one.

THERMOMETER BRIDGE ACCURACY – It is provided by the manual of the thermometer reading instrument. In this case a triangular probability distribution function has been used.

SPRT SELF-HEATING - The calibration certificate provides the value of the heating effect due to the passage of a current of 1 mA through the SPRT, in terms of increase of the thermometer resistance value at the triple point of water, R_0 . The increase of the resistance, ΔR , is 138 $\mu\Omega$, that in terms of temperature ΔT becomes 0.00136 °C, considering that $\Delta T = \Delta R / (\alpha \cdot R_0)$ where α is the thermal expansion coefficient of platinum. Considering a rectangular asymmetric probability distribution, the uncertainty contribution to T_{tp} of the SPRT self-heating is obtained as:

$$u(T) = \frac{\Delta T}{\sqrt{3}}$$

SPRT DRIFT – The SPRT manual specifies that the temperature drift of the thermometer over a year is about 0.001 °C.

PRESSURE DROP – this value is the gas pressure difference between the saturator out let and the CMH or CRDS inlet. The total pressure drop is 120 Pa with asymmetric rectangular probability distribution function. So the standard uncertainty is 69 Pa.

LONG TERM STABILITY OF THE PRESSURE GAUGE- According to the device manual the long term stability of the pressure gauge is 0.01 % of the full scale per year, thus the contribution to the uncertainty becomes 26.2 Pa/year.

BAROMETER RESOLUTION AND ACCURACY - In the device catalogue the resolution is 0.1 Pa and the accuracy is the 0.05 % of the full scale range of the device capability which corresponds to 131 Pa.

Type A evaluation has been applied to evaluate the uncertainty contribution to $u(T_{fp})$ for the following components:

SATURATION TEMPERATURE STABILITY – After monitoring the outlet gas temperature and considering normal distribution function the standard uncertainty is calculated by Eq. (5, 6).

SATURATOR TEMPERATURE UNIFORMITY- It is the gradient of temperature along the saturator. A rectangular distribution function is considered.

SATURATOR EFFICIENCY – This term is measured by calculating the x_w and T_{fp} by varying the flow rate \emptyset between $1.5 \text{ l}\cdot\text{min}^{-1}$ and $7 \text{ l}\cdot\text{min}^{-1}$. Here the probability distribution function is rectangular.

SATURATION PRESSURE STABILITY - After monitoring the outlet gas pressure and considering normal distribution function the standard uncertainty is calculated by Eq. (5, 6).

In the water vapour mole fraction, $x_w = \frac{e_w(T)f(T,P)}{P}$, the uncertainty of the humid gas generated by the low frost-point generator can be evaluated considering the contributions of the pressure measurement P , saturation vapour pressure $e_w(T)$ where is calculated by the Sonntag formulation (Eq.7), ²⁴ and the enhancement factor $f(T, P)$ computed based on the Greenspan's equation (Eq.9). ²⁵

The combined uncertainty if there isn't any correlation between influence quantities is the square root of the sum of the squares of each contribution uncertainty weighted for its own sensitivity coefficient (Eq.3).

According to the Sonntag equation, the saturation pressure and its' standard uncertainty can be expressed as:

$$\ln(e_w) = \sum_{i=0}^3 g_i T^{i-1} + g_4 \ln(T) \quad (7)$$

$$u(e_w) = \frac{de_w}{dT} * u_c(T) \quad (8)$$

In this equation T is the working temperature expressed in kelvin, g_i , and g_4 are the constants are for saturation pressure over the ice (table 5.1). The term $u_i(T)$ is the frost point combined uncertainty.

g_0	g_1	g_2	g_3	g_4
-6024.5282	29.32707	1.0613868×10^{-2}	$-1.3198825 \times 10^{-5}$	-0.49382577

Table 5.1. The constants of the Sonntag equation for saturation pressure over the ice.

The enhancement factor $f(T, P)$ is calculated by the following equation which is Greenspan's formula: ²⁵

$$f(T, P) = \exp(\alpha(T) \left[1 - \frac{e_w}{P}\right] + \beta(T) \left[\frac{P}{e_w} - 1\right]) \quad (8)$$

In this equation the T and P are the measured frost point temperature is expressed in kelvin and the saturation pressure in pascal. $\alpha(T)$ and $\beta(T)$ are calculated as :

$$\alpha(T) = \sum_{i=1}^4 A_i T^{i-1}, \quad \beta(T) = \exp\left[\sum_{i=1}^4 B_i T^{i-1}\right]$$

The values of A_i and B_i are reported in the table 5.2 and 5.3.

A_1	A_2	A_3	A_4
$-7.4712663 \times 10^{-2}$	9.5972907×10^{-4}	$-4.1935419 \times 10^{-6}$	6.2038841×10^{-9}

Table 5.2. The values of A_i in the Greenspan's equation.

B_1	B_2	B_3	B_4
$-8.2308868 \times 10^{-1}$	5.6519110×10^{-1}	$-1.5304505 \times 10^{-3}$	1.5395086

Table 5.3. The values of B_i in the Greenspan's equation.

The uncertainty of the enhancement factor $u(f)$ is evaluated by the Lowell-Smith formula as the following equation: ²⁶

$$u_r(f) = (a_0 P + a_1) \exp([a_2 \ln(P) + a_3]T) \quad (9)$$

$$u(f) = f * u_r(f) \quad (10)$$

where $u_r(f)$ – relative uncertainty, T, P – working temperature and pressure measured in Celsius and pascal. The constant a_0, a_1, a_2 , and a_3 value are reported in table 5.4.

a_0	a_1	a_2	a_3
1.68×10^{-3}	-1×10^{-5}	2.2×10^{-5}	-0.0136

Table 5.4. The Lovell-Smith uncertainty analysis constants value.

Now the combined uncertainty will be as:

$$u_c(x_w) = \sqrt{\left(\frac{dx_w}{d(e_w(T))}\right)^2 u(e_w)^2 + \left(\frac{dx_w}{dP}\right)^2 u(P)^2 + \left(\frac{dx_w}{df(T, P)}\right)^2 u(f)^2} \quad (11)$$

So after computing the derivatives the equation will be :

$$u(x_w) = \sqrt{\left(\frac{f}{P} \frac{de_w}{dT}\right)^2 (u_c(T))^2 + \left(\frac{e_w f}{P^2}\right)^2 u(P)^2 + \left(\frac{e_w}{P}\right)^2 u(f)^2} \quad (12)$$

here $u(P)$ is the standard deviation of the measured pressure.

In table 5.5, 5.6, 5.7, and 5.8 all source of the uncertainty and their sensitivity coefficient for the frost-point T_{fp} and water vapour mole fraction x_w is reported. The final result of each table is the combined uncertainty which is the square root of the sum of the squares of each term multiplies by the sensitivity coefficient is calculated. For example in table 5.5 the combined uncertainty of the frost-point $u_c(T_{fp})$ at $T_{fp} = -75$ °C and $P = 1100$ hPa is 0.074 °C and the water vapour mole fraction combined uncertainty $u_c(x_w)$ is $1.32 \cdot 10^{-8}$. The other uncertainty analysis can be find in the Appendix.

Source	Standard uncertainty	Probability distribution function	sensitivity coefficient	Contribution to Standard uncertainty/ °C
Saturation temperature stability	0.0008°C	Normal	1	0.0008
Sat temperature uniformity	0.0004°C	Rectangular	1	0.0004
SPRT calibration	0.00025°C	Normal	1	0.00025
Thermal bridge accuracy	0.00061°C	Triangular	1	0.00061
Self-heating SPRT	0.000786 Ω	Asymmetric Rectangular	9.8640 °C Ω ⁻¹	0.00775
SPRT drift/year	0.001 °C	rectangular	1	0.000577
Saturation EFFICIENCY	0.0736°C	Rectangular	1	0.0736
Pressure drop	69 Pa	Rectangular asymmetric	0.000033 °C Pa	0.0023
Combined uncertainty, u_c				0.074

Table 5.5. Saturator uncertainty budget on the frost-point temperature T_{fp} when nominally $T_{fp} = -75$ °C and $P = 1100$ hPa

Source	Standard uncertainty	Probability distribution function	sensitivity coefficient	Contribution to Standard uncertainty / mol mol ⁻¹
Pure water vapour saturation pressure, $e(T_{fp})$	0.0014 Pa	Normal	9.17×10^{-6}	1.43×10^{-6}
enhancement factor, $f(T_{fp}, P)$	0.0004 mol mol ⁻¹	Normal	1.13×10^{-6}	5.52×10^{-10}
saturator pressure, P	9.76 Pa	Normal	1×10^{-11}	1.01×10^{-10}
Combined uncertainty, u_c				1.32×10^{-8}

Table 5.6. Water vapour mole fraction uncertainty budget, when nominally $x_w = 1 \cdot 10^{-6}$ mol·mol⁻¹ ($T_{fp} = -75$ °C and $P = 1100$ hPa)

Source	Standard uncertainty	Probability distribution function	sensitivity coefficient	Contribution to Standard uncertainty/ °C
Saturation temperature stability	0.0779 °C	Normal	1	0.0779
Sat temperature uniformity	0.0939 °C	Rectangular	1	0.0939
SPRT calibration	0.00025 °C	Normal	1	0.00025
Thermal bridge accuracy	0.00061 °C	Triangular	1	0.00061
Self-heating SPRT	0.000786 Ω	Asymmetric Rectangular	9.8640 °C Ω ⁻¹	0.00775
SPRT drift/year	0.001 °C	Rectangular	1	0.000577
Saturation EFFICIENCY	0.289 °C	Rectangular	1	0.289
Pressure drop	69 Pa	Rectangular asymmetric	0.000 027	0.0019
Combined uncertainty, u_c				0.314

Table 5.7. Saturator uncertainty budget on the frost-point temperature T_{fp} when nominally $T_{fp} = -95$ °C and $P = 1100$ hPa

Source	Standard uncertainty	Probability distribution function	sensitivity coefficient	Contribution to Standard uncertainty / mol mol ⁻¹
Pure water vapour saturation pressure, $e(T_{fp})$	0.00022	Normal	9.19×10^{-6}	2.57×10^{-9}
enhancement factor, $f(T_{fp}, P)$	6.49×10^{-4} mol mol ⁻¹	Normal	3.35×10^{-8}	2.17×10^{-11}
saturated pressure, P	6.17 Pa	Normal	3.084×10^{-13}	1.9×10^{-12}
Combined uncertainty, u_c				2.05×10^{-9}

Table 5.8. Water vapour mole fraction uncertainty budget, when nominally $x_w = 34 \times 10^{-9}$ mol·mol⁻¹ ($T_{fp} = -95$ °C, $P = 1100$ hPa)

6. Conclusions

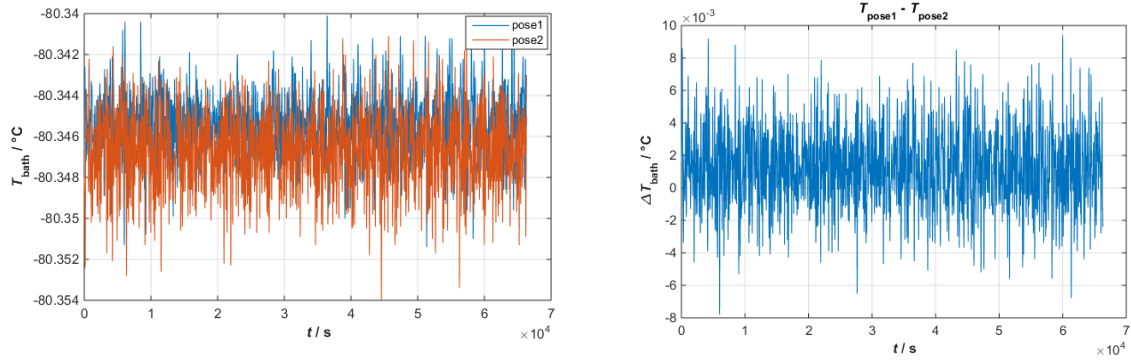
The analysis of water vapor impurity is important in a number of cutting-edge technology, fields such as the semiconductor manufacturing process, display industry, and gas industry. The sensing of trace-moisture in gases, with an amount of substance fraction less than $1 \mu\text{mol mol}^{-1}$, has become increasingly important in the recent decade, because it has been recognized that even such a small amount of water vapor plays a critical role in the yield and product quality. International Vocabulary of Metrology (VIM) defined Metrological Traceability that is a property of a measurement result whereby the result can be related to a reference through a documented unbroken chain. When reporting the result of a measurement of a physical quantity, it is obligatory that some quantitative indication of the quality of the result be given to comparing the result, either among themselves or with reference values. It is therefore necessary that there be a readily implemented, easily understood, and generally accepted procedure for characterizing the quality of a result of a measurement, that is, for evaluating and expressing its uncertainty.

There are many analytical methods for determination of trace water vapor which all require regular, traceable calibration. Humidity can be fully described with a single parameter if the gas pressure and temperature are known. So, many national humidity laboratories have chosen the dew-point temperature as the primary humidity parameter. As the realization of a dew-point temperature scale, a dew-point generator provides a simple source of traceability in a wide range at good uncertainty level. INRIM03 is a novel humidity standard, an ultra-low frost-point generator which developed to extend the Italian humidity calibration measurement capabilities down to few parts per billions of water. The system object of this thesis can generate a humid gas flow with an amount of water down to tens parts per billions. This generator is among the few ones in the world able to work at frost point temperatures down to $-95 \text{ }^\circ\text{C}$ and at sub-atmospheric pressures (200 hPa) independent of the gas flow rate, the inlet gas flow rate \emptyset

which is varying from 1.5 l min^{-1} to 7 l min^{-1} . The result of the thesis will be published as uncertainty budget for frost point temperature T_{fp} and water vapour mole fraction, x_w , generated by the generator. The design was tested in order to guarantee the stability of temperature and pressure. By varying flow rate and inlet dry gas, the generator efficiency is examined. Also, after changing step-by-step the pressure and temperature the performance of the system is monitored. The uncertainty analysis for all the temperature and pressure was done. The final combined for the uncertainty severe condition ($T_{\text{fp}} = -95 \text{ }^\circ\text{C}$ at atmospheric pressure) is $u_c(T_{\text{fp}}) = 0.314 \text{ }^\circ\text{C}$ and $u_c(x_w) = 2.11 \times 10^{-9} \text{ mol mol}^{-1}$.

Appendix

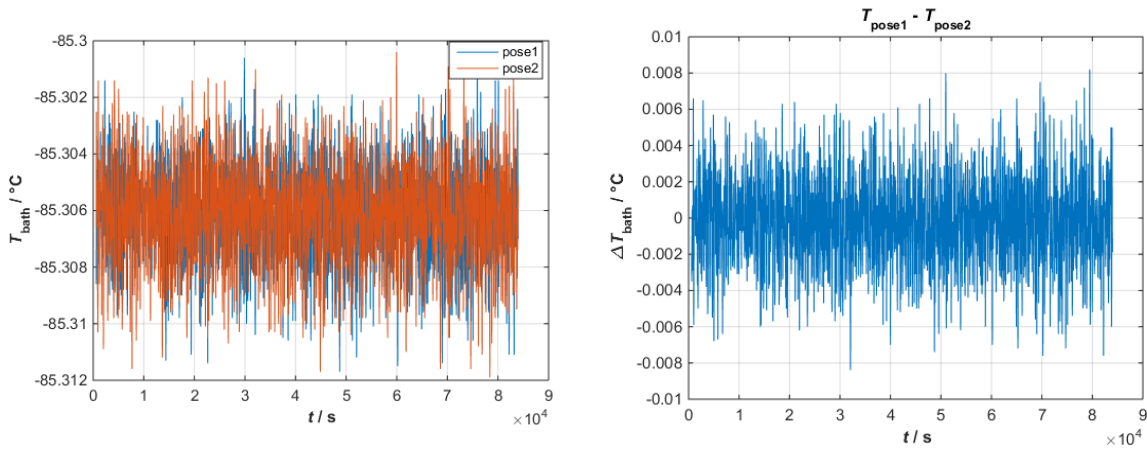
A.1 Bath temperature stability



a)

b)

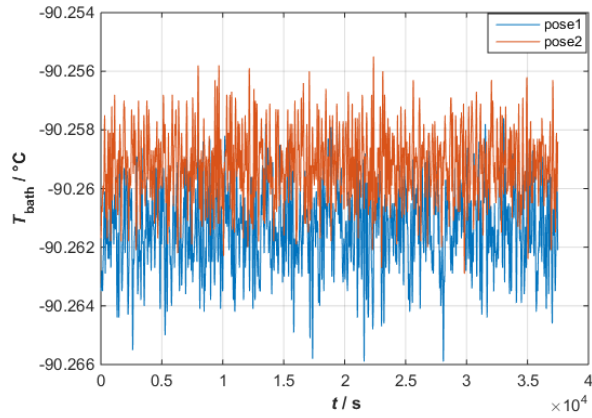
Figure A.1. a) Measurement of the saturator temperature at two different depths as a function of the time for a nominal $T_{\text{sat}} = -80 \text{ } ^\circ\text{C}$ and $P = 1100 \text{ hPa}$. The red line represents pose 1 temperature, the blue one is the saturator temperature at pose 2; b) Uniformity of the saturator temperature, ΔT , as a function of the time. It is determined by the difference between the two temperature.



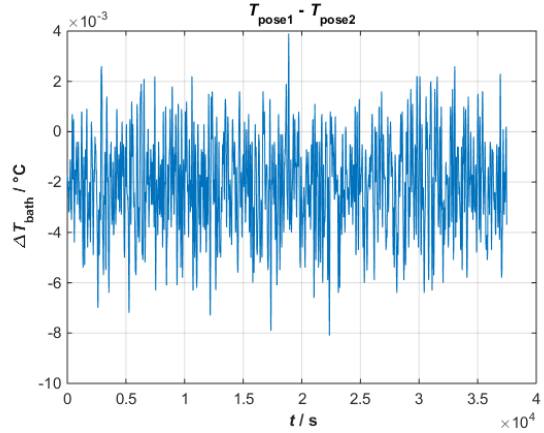
a)

b)

Figure A.2. a) Measurement of the saturator temperature at two different depths as a function of the time for a nominal $T_{\text{sat}} = -85 \text{ } ^\circ\text{C}$ and $P = 1100 \text{ hPa}$. The red line represents pose 1 temperature, the blue one is the saturator temperature at pose 2; b) Uniformity of the saturator temperature, ΔT , as a function of the time. It is determined by the difference between the two temperature.

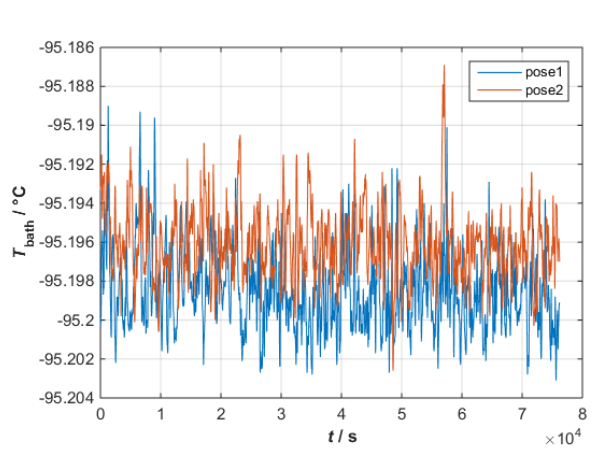


a)

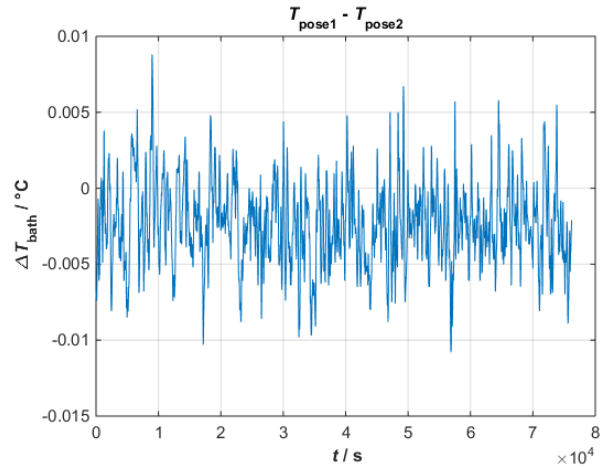


b)

Figure A.3. a) Measurement of the saturator temperature at two different depths as a function of the time for a nominal $T_{\text{sat}} = -90$ °C and $P = 1100$ hPa. The red line represents pose 1 temperature, the blue one is the saturator temperature at pose 2; b) Uniformity of the saturator temperature, ΔT , as a function of the time. It is determined by the difference between the two temperature.



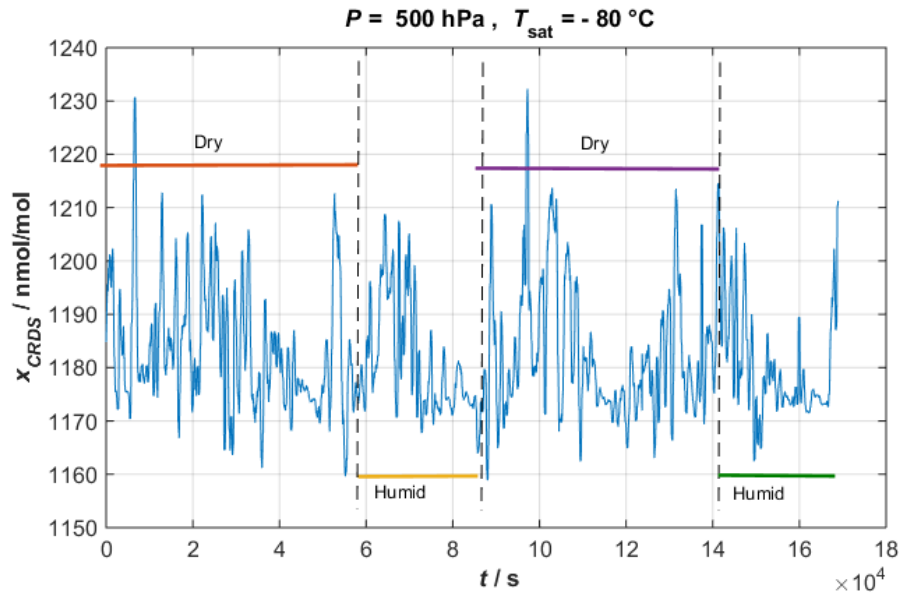
a)



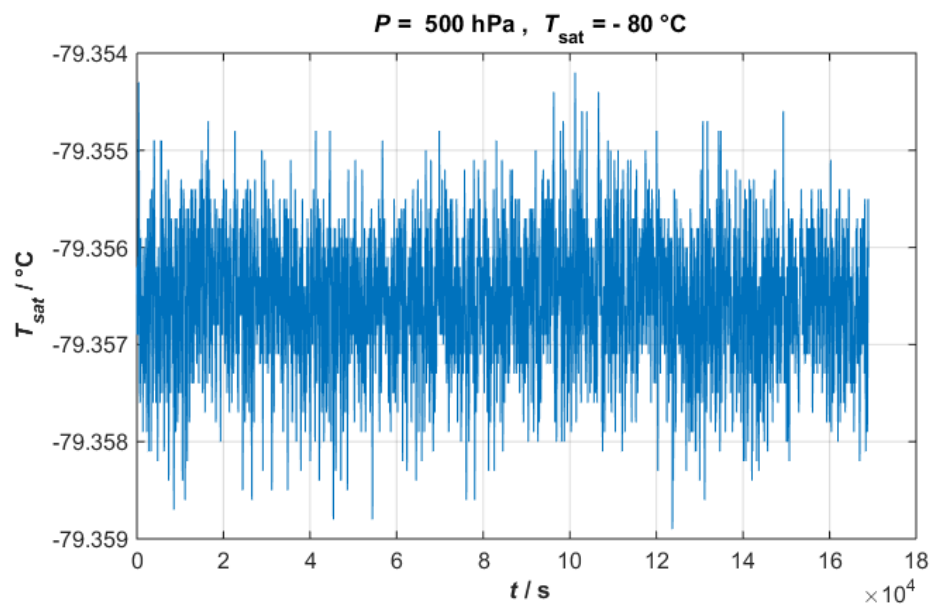
b)

Figure A.4. a) Measurement of the saturator temperature at two different depths as a function of the time for a nominal $T_{\text{sat}} = -95$ °C and $P = 1100$ hPa. The red line represents pose 1 temperature, the blue one is the saturator temperature at pose 2; b) Uniformity of the saturator temperature, ΔT , as a function of the time. It is determined by the difference between the two temperature.

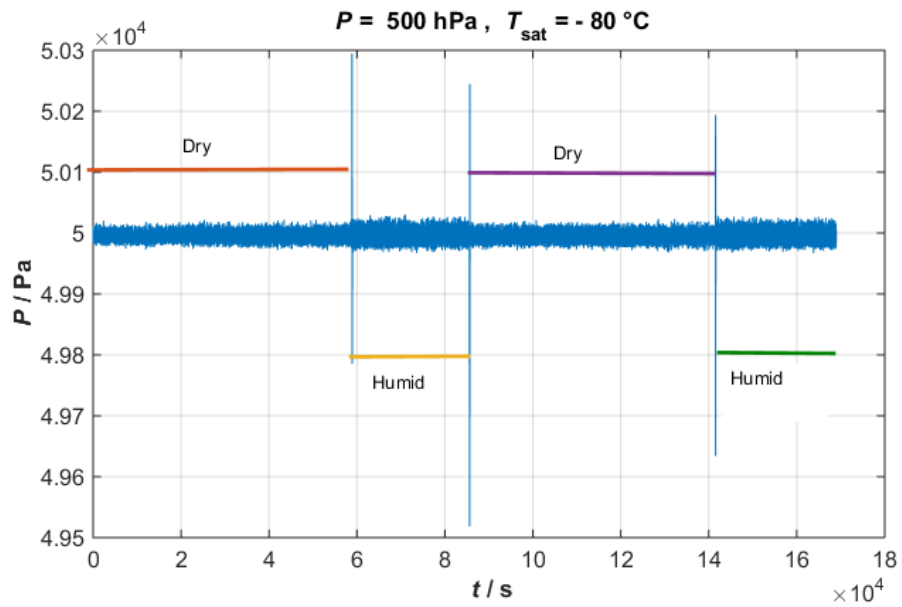
A.2 Experimental results of generator efficiency



a)

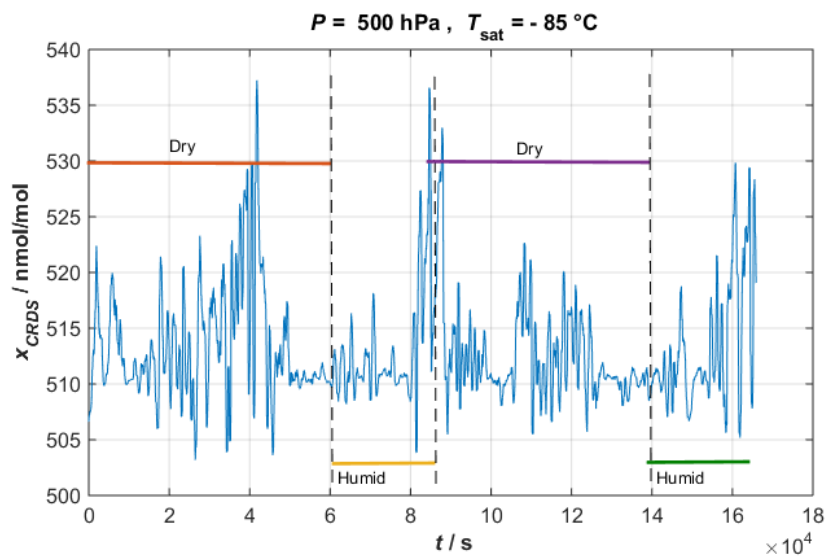


b)

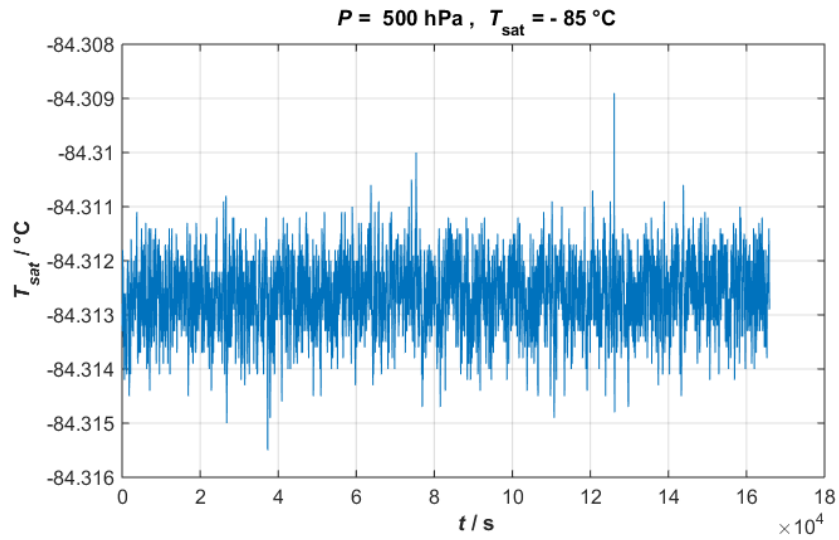


c)

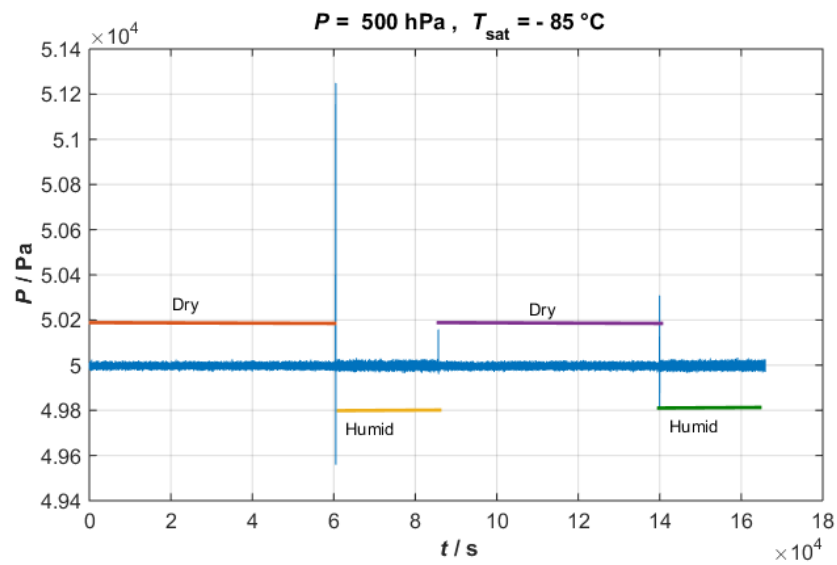
Figure A.5. Alternating the inlet gas when $T_{\text{sat}} = -80\text{ °C}$, $P = 500\text{ hPa}$. Variation of the water vapour mole fraction measured by CRDS (a), of the saturated gas temperature measure by SPRT(b) , and pressure stability by varying the inlet gas from humid to dry(c)



a)

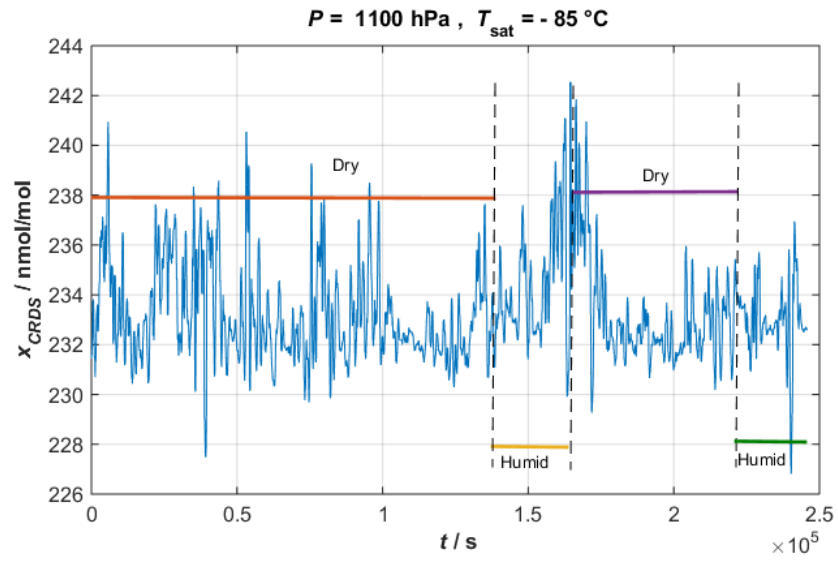


b)

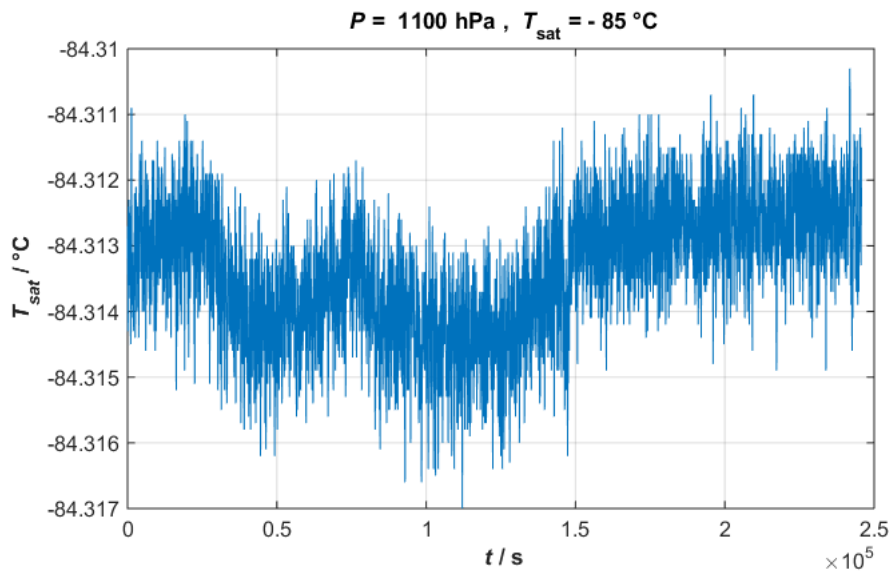


c)

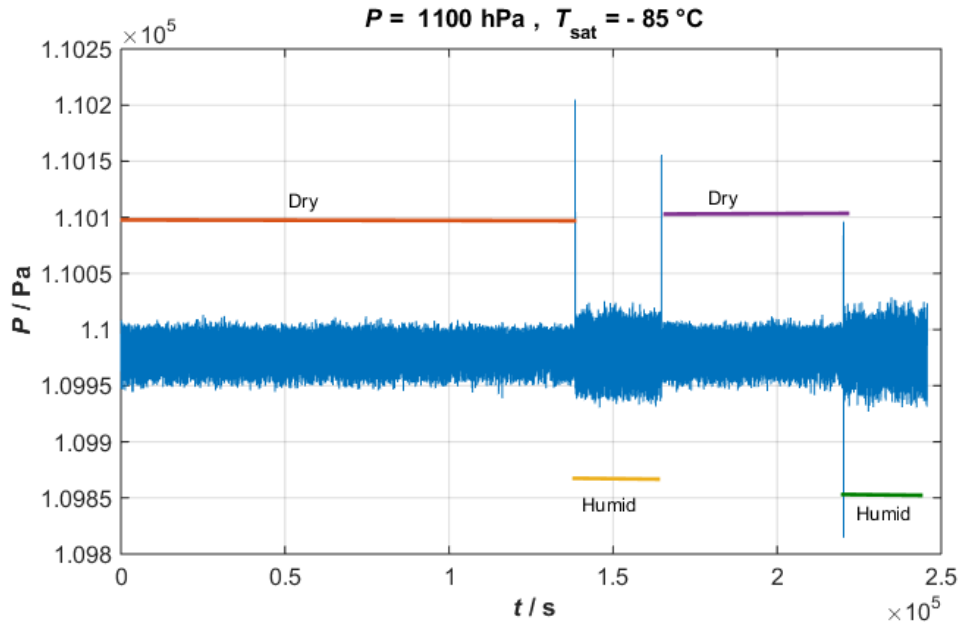
Figure A.6. Alternating the inlet gas when $T_{\text{sat}} = -85\text{ °C}$, $P = 500\text{ hPa}$. Variation of the water vapour mole fraction measured by CRDS (a), of the saturated gas temperature measure by SPRT(b) , and pressure stability by varying the inlet gas from humid to dry(c)



a)



b)



c)

Figure A.7. Alternating the inlet gas when $T_{\text{sat}} = -85 \text{ }^\circ\text{C}$, $P = 1100 \text{ hPa}$. Variation of the water vapour mole fraction measured by CRDS (a), of the saturated gas temperature measure by SPRT(b), and pressure stability by varying the inlet gas from humid to dry(c).

A.3 Uncertainty analysis

Source	Standard uncertainty	Probability distribution function	sensitivity coefficient	Contribution to Standard uncertainty/ °C
Saturation temperature stability	0.00079 °C	Normal	1	0.00079
Sat temperature uniformity	0.0004 °C	Rectangular	1	0.0004
SPRT calibration	0.00025 °C	Normal	1	0.00025
Thermal bridge accuracy	0.00061 °C	Triangular	1	0.00061
Self-heating SPRT	0.000786 Ω	Asymmetric Rectangular	9.8640 °C Ω ⁻¹	0.00775
SPRT drift/year	0.001 °C	Rectangular	1	0.000577
Saturation EFFICIENCY	0.4313 °C	Rectangular	1	0.4313
Pressure drop	69 Pa	Rectangular asymmetric	0.000 027 °C Pa ⁻¹	0.0018
Combined uncertainty, u_c				0.4314

Table A.1, frost-point temperature uncertainty budget, $T_{\text{sat}} = -75$ °C, $P = 200$ hPa)

Source	Standard uncertainty	Probability distribution function	sensitivity coefficient	Contribution to Standard uncertainty / mol mol ⁻¹
Pure water vapour saturation pressure, $e(T_{\text{fp}})$	0.0084 Pa	Normal	5.00664×10^{-5}	4.19×10^{-7}
enhancement factor, $(f(T_{\text{fp}}, P))$	6.57×10^{-5} mol mol ⁻¹	Normal	6.21×10^{-6}	4.08×10^{-10}
saturated pressure, P	10.39 Pa	Normal	3.11×10^{-10}	3.23×10^{-9}
Combined uncertainty, u_c				4.19×10^{-7}

Table A.2, water vapour mole fraction uncertainty budget, when nominally $x_w = 1.5 \times 10^{-6}$ mol mol⁻¹ ($T_{\text{sat}} = -75$ °C, $P = 200$ hPa)

Source	Standard uncertainty	Probability distribution function	sensitivity coefficient	Contribution to Standard uncertainty/ °C
Saturation temperature stability	0.0012 °C	Normal	1	0.0012
Sat temperature uniformity	0.0029 °C	Rectangular	1	0.0029
SPRT calibration	0.00025 °C	Normal	1	0.00025
Thermal bridge accuracy	0.00061 °C	Triangular	1	0.00061
Self-heating SPRT	0.000786 Ω	Asymmetric Rectangular	9.8640 °C Ω ⁻¹	0.00775
SPRT drift/year	0.001 °C	Rectangular	1	0.000577
Saturation EFFICIENCY	0.3791 °C	Rectangular	1	0.3791
Pressure drop	69 Pa	Rectangular asymmetric	0.00007 °C Pa ⁻¹	0.0048
Combined uncertainty, u_c				0.098

Table A.3, frost-point temperature uncertainty budget, $T_{\text{sat}} = -80$ °C, $P = 500$ hPa

Source	Standard uncertainty	Probability distribution function	sensitivity coefficient	Contribution to Standard uncertainty / mol mol ⁻¹
Pure water vapour saturation pressure, $e(T_{\text{fp}})$	4.60×10^{-6} Pa	Normal	2.00×10^{-5}	9.24×10^{-11}
enhancement factor, $(f(T_{\text{fp}}, P))$	2.38×10^{-4} mol mol ⁻¹	Normal	4.47×10^{-7}	1.06×10^{-10}
saturated pressure, P	15.85 Pa	Normal	8.97×10^{-12}	1.42×10^{-10}
Combined uncertainty, u_c				1.68×10^{-8}

Table A.4, water vapour mole fraction uncertainty budget, when nominally $x_w = 1.09 \times 10^{-6}$ mol mol⁻¹ ($T_{\text{sat}} = -80$ °C, $P = 500$ hPa)

Source	Standard uncertainty	Probability distribution function	sensitivity coefficient	Contribution to Standard uncertainty/ °C
Saturation temperature stability	0.0014 °C	Normal	1	0.0014
Sat temperature uniformity	0.0029 °C	Rectangular	1	0.0029
SPRT calibration	0.00025 °C	Normal	1	0.00025
Thermal bridge accuracy	0.00061 °C	Triangular	1	0.00061
Self-heating SPRT	0.000786 Ω	Asymmetric Rectangular	9.8640 °C Ω ⁻¹	0.00775
SPRT drift/year	0.001 °C	Rectangular	1	0.000577
Saturation EFFICIENCY	0.1017 °C	Rectangular	1	0.1017
Pressure drop	69 Pa	Rectangular asymmetric	0.00004 °C Pa ⁻¹	0.0028
Combined uncertainty, u_c				0.102

Table A.5, frost-point temperature uncertainty budget, $T_{\text{sat}} = -85$ °C, $P = 800$ hPa

Source	Standard uncertainty	Probability distribution function	sensitivity coefficient	Contribution to Standard uncertainty / mol mol ⁻¹
Pure water vapour saturation pressure, $e(T_{\text{fp}})$	0.0004 Pa	Normal	1.28×10^{-5}	5×10^{-9}
enhancement factor, $(f(T_{\text{fp}}, P))$	4.01×10^{-4} mol mol ⁻¹	Normal	2.80×10^{-7}	1.12×10^{-10}
saturated pressure, P	16.52 Pa	Normal	3.51×10^{-12}	5.80×10^{-11}
Combined uncertainty, u_c				5×10^{-9}

Table A.6, water vapour mole fraction uncertainty budget, when nominally $x_w = 295 \times 10^{-9}$ mol mol⁻¹ ($T_{\text{sat}} = -85$ °C, $P = 800$ hPa)

Source	Standard uncertainty	Probability distribution function	sensitivity coefficient	Contribution to Standard uncertainty/ °C
Saturation temperature stability	0.0006 °C	Normal	1	0.0006
Sat temperature uniformity	0.0008 °C	Rectangular	1	0.0008
SPRT calibration	0.00025 °C	Normal	1	0.00025
Thermal bridge accuracy	0.00061 °C	Triangular	1	0.00061
Self-heating SPRT	0.00078 Ω	Asymmetric Rectangular	9.8640 °C Ω ⁻¹	0.00775
SPRT drift/year	0.001 °C	Rectangular	1	0.000577
Saturation EFFICIENCY	0.07331	Rectangular	1	0.07331
Pressure drop	69 Pa	Rectangular asymmetric	0.00004°C Pa ⁻¹	0.0027
Combined uncertainty, u_c				0.0737

Table A.7, frost-point temperature uncertainty budget, $T_{\text{sat}} = -90$ °C, $P = 800$ hPa)

Source	Standard uncertainty	Probability distribution function	sensitivity coefficient	Contribution to Standard uncertainty / mol mol ⁻¹
Pure water vapour saturation pressure, $e(T_{\text{fp}})$	0.00015 Pa	Normal	1.26×10^{-5}	1.86×10^{-9}
enhancement factor, $(f(T_{\text{fp}}, P))$	4.30×10^{-4} mol mol ⁻¹	Normal	1.38×10^{-7}	5.94×10^{-11}
saturated pressure, P	15.54 Pa	Normal	1.74×10^{-12}	2.70×10^{-11}
Combined uncertainty, u_c				1.86×10^{-9}

Table A.8, water vapour mole fraction uncertainty budget, when nominally $x_w = 121 \times 10^{-9}$ molmol⁻¹ ($T_{\text{sat}} = -90$ °C, $P = 800$ hPa)

Source	Standard uncertainty	Probability distribution function	sensitivity coefficient	Contribution to Standard uncertainty/ °C
Saturation temperature stability	0.00070 °C	Normal	1	0.00070
Sat temperature uniformity	0.0004 °C	Rectangular	1	0.0004
SPRT calibration	0.00025 °C	Normal	1	0.00025
Thermal bridge accuracy	0.00061 °C	Triangular	1	0.00061
Self-heating SPRT	0.000786 Ω	Asymmetric Rectangular	9.8640 °C Ω ⁻¹	0.00775
SPRT drift/year	0.001 °C	Rectangular	1	0.000577
Saturation EFFICIENCY	0.0882 °C	Rectangular	1	0.0882
Pressure drop	69 Pa	Rectangular asymmetric	0.00015 °C Pa ⁻¹	0.0102
Combined uncertainty, u_c				0.089

Table A.9, frost-point temperature uncertainty budget, $T_{\text{sat}} = -95$ °C, $P = 200$ hPa)

Source	Standard uncertainty	Probability distribution function	sensitivity coefficient	Contribution to Standard uncertainty / mol mol ⁻¹
Pure water vapour saturation pressure, $e(T_{\text{fp}})$	0.000062 Pa	Normal	5.00251×10^{-5}	3.14×10^{-9}
enhancement factor, $f(T_{\text{fp}}, P)$	8.69×10^{-5} mol mol ⁻¹	Normal	1.81849×10^{-7}	1.58×10^{-11}
saturated pressure, P	11.6173 Pa	Normal	9.09701×10^{-12}	1.06×10^{-10}
Combined uncertainty, u_c				3.14×10^{-9}

Table A.10, water vapour mole fraction uncertainty budget, when nominally $x_w = 189 \times 10^{-9}$ molmol⁻¹ ($T_{\text{sat}} = -95$ °C, $P = 200$ hPa)

References

1. Martti Heinonen, Mittatekniikan keskus. *Uncertainty in humidity measurements Publication of theEUROMET Workshop P758*. ISSN 1235-2704
2. Dario Camuffo, Chiara Bertolin ,Arianna Bergonzini, Chiara Amore , Claudio Cocheo. *Early hygrometric observations in Padua, Italy, from 1794 to 1826*. Climatic Change (2014) 122:217–227
3. Wilhelm van Schaik, Mart Grooten, Twan Wernaart, Cees van der Geld. *High Accuracy Acoustic Relative Humidity Measurement in Duct Flow with Air*. 7421-7433
4. Yankee Environmental Systems, INC. Airport industrial park.
5. Ashis Tripathy , Sumit Pramanik, Jongman Cho, Jayasree Santhosh, and Noor Azuan Abu Osman. *Role of Morphological Structure, Doping, and Coating of Different Materials in the Sensing Characteristics of Humidity Sensors*, ISSN 1424-8220.
6. Chia-Yen Lee, Gwo-Bin Lee. *Humidity Sensors*. Sensor Letters 2005, 3, 1–14
7. Piotr Zalicki, Richard N.Zare, *Cavity ring-down spectroscopy for quantitative absorption measurements*.
8. R. Buchhold, A. Nakladal, G. Gerlach, P. Neumann. *Design studies on piezoresistive humidity sensors*. Sensors and Actuators B 53 (1998) 1–7
9. International Bureau of Weights and Measures (20 May 2019), SI Brochure: The International System of Units (SI) (9th ed.)ISBN 978-92-822-2272-0
10. Pieter R. Wiederhold. *Watre vapour measurement methods and instrumentation*.
11. C W Meyer, J T Hodges, R W Hyland, G E Scace, J Valencia-Rodriguez, and J R Whetstone. *The second-generation NIST standard hygrometer*. Metrologia 47 (2010) 192–207
12. Bell, S.A. (1995). *Validation of the NPL gravimetric hygrometer*. (Unpublished Doctoral thesis, City University London)
13. C.W. Meyer,J.T. Hodges,P.H. Huang,W.W. Miller,D.C. Ripple,G.E. Scace. *Calibration of Hygrometers with the Hybrid Humidity Generator*. NIST SP 250-83.

14. Mohamed Gamal Ahmed, Said Mazen, Doaa Abd El-Gelil and Nabila Ismail El Sayed. *Realization of Relative Humidity Scale Using NIS Two-Temperature Humidity Generator*. 4 (8) (2014) 484-487
15. Doaa Mohamed Abd El-Galil and Essam Mahmoud. *NIS two-pressure humidity generator*. Qual. Eng. 7, 303 (2016).
16. Hisashi Abe, Hiroshi Kitano. *Development of humidity standard in trace-moisture region: Characteristics of humidity generation of diffusion tube humidity generator*. Sensors and Actuators A 128 (2006) 202–208.
17. Kanolt, C. W. *Bureau of Standards Sci. Papers* 520, Vol. 20,p. 619 (1926).
18. G. Mamontov, D. Mamontova, and L. Konopelko. *Realization of the phase equilibrium method in the standard low frost point humidity generator*
19. B. I. Choi , H. S. Nham , S. B. Woo , J. C. Kim , S. Y. Kwon. *The New KRISS Low Frost-Point Humidity Generator*. 29:1578–1588
20. B. I. Choi, S.-W. Lee, J. C. Kim, S. B. Woo. *Extension of humidity standards to –105 °C Frost Point*. 36:2231–2241
21. Andrea Peruzzi. *Primary Standards for Humidity*, Delft, 18 September 2007.
22. R Cuccaro, L Rosso , D Smorgon , G Beltramino , S Tabandeh ,and V Fernicola. *Development of a low frost-point generator operating at sub-atmospheric pressure*. 2018 Meas. Sci. Technol.29 054002
23. *Evaluation of measurement data, Guide to the expression of uncertainty in measurement*, JCGM 100:2008
24. Sonntag D 1990 *Important new values of the physical constants of 1986, vapor pressure formulations based on the ITS–90, and psychrometer formulae* Z. Meteorol. 40 304-4
25. Greenspan L 1976 *Functional equations for the enhancement factors for CO₂-free moist air* J. Res. Natl Bur. Stand. 80A 41-4
26. Lovell-Smith J 2009 *The propagation of uncertainty for humidity calculations*. Metrologia 46 607-15